2007-03

Vertical variation of dust and its impact on the top of the atmosphere brightness temperature in the midwave infrared

Lucyk, Paul W.

Monterey California. Naval Postgraduate School

NAVAL POSTGRADUATE SCHOOL

MONTEREY, CALIFORNIA

THESIS

VERTICAL VARIATION OF DUST AND ITS IMPACT ON THE TOP OF THE ATMOSPHERE BRIGHTNESS TEMPERATURE IN THE MIDWAVE INFRARED

by

Paul W. Lucyk

March 2007

Thesis Advisor:	Philip A. Durkee
Second Reader:	Kurt Nielsen

Approved for public release; distribution is unlimited

THIS PAGE INTENTIONALLY LEFT BLANK

REPORT DOCUMENTATION PAGE		Form Approved OMB No. 0704-0188

1. AGENCY USE ONLY *(Leave blank)*	2. REPORT DATE	3. REPORT TYPE AND DATES COVERED
	March 2007	Master's Thesis

4. TITLE AND SUBTITLE Vertical Variation of Dust and Its Impact on the Top of the Atmosphere Brightness Temperature in the Midwave Infrared	5. FUNDING NUMBERS
6. AUTHOR(S) Paul W. Lucyk	
7. PERFORMING ORGANIZATION NAME(S) AND ADDRESS(ES) Naval Postgraduate School Monterey, CA 93943-5000	8. PERFORMING ORGANIZATION REPORT NUMBER
9. SPONSORING /MONITORING AGENCY NAME(S) AND ADDRESS(ES) N/A	10. SPONSORING/MONITORING AGENCY REPORT NUMBER

11. SUPPLEMENTARY NOTES The views expressed in this thesis are those of the author and do not reflect the official policy or position of the Department of Defense or the U.S. Government.

12a. DISTRIBUTION / AVAILABILITY STATEMENT	12b. DISTRIBUTION CODE
Approved for public release; distribution is unlimited	

13. ABSTRACT (maximum 200 words)

The objective of this thesis is to investigate the vertical distribution of dust and its impact on the top of the atmosphere radiance and associated remotely sensed thermal variability in the midwave infrared wavelengths. Due to the inconsistent availability and coincidence of in-situ data with dust events, model data was used to identify the vertical dust regions. The Navy Aerosol Analysis and Prediction System global aerosol model was used to determine mass concentration and vertical extent of dust. Mass concentration was converted to extinction and individual dust events were analyzed to characterize the vertical distribution, extinction, and optical depth. The average height was defined for specific dust regions of Iraq and Korea. This value was used to determine the impact of the dust layer on the top of the atmosphere radiance and brightness temperature in the wavelengths of interest. Radiative transfer software was used to determine the top of the atmosphere radiance of the modeled dust atmosphere. Resultant brightness temperature was calculated to obtain the thermal characteristics of the dust layer and associated atmosphere. The vertical distribution of the dust layer was varied with fixed atmospheric components to gain insight into the resultant variation of radiance and subsequent brightness temperature to provide a set of possible values for a regionally specific dust event.

14. SUBJECT TERMS Dust, Aerosol, Midwave Infrared, Vertical Variation, Radiance, Brightness Temperature	15. NUMBER OF PAGES 89
	16. PRICE CODE

17. SECURITY CLASSIFICATION OF REPORT	18. SECURITY CLASSIFICATION OF THIS PAGE	19. SECURITY CLASSIFICATION OF ABSTRACT	20. LIMITATION OF ABSTRACT
Unclassified	Unclassified	Unclassified	UL

NSN 7540-01-280-5500 Standard Form 298 (Rev. 2-89)
Prescribed by ANSI Std. 239-18

THIS PAGE INTENTIONALLY LEFT BLANK

Approved for public release; distribution is unlimited

VERTICAL VARIATION OF DUST AND ITS IMPACT ON THE TOP OF THE ATMOSPHERE BRIGHTNESS TEMPERATURE IN THE MIDWAVE INFRARED

Paul W. Lucyk
Captain, United States Air Force
B.S., Florida State University, 1999

Submitted in partial fulfillment of the
requirements for the degree of

MASTER OF SCIENCE IN METEOROLOGY

from the

NAVAL POSTGRADUATE SCHOOL
March 2007

Author: Paul W. Lucyk

Approved by: Philip A. Durkee
Thesis Advisor

Kurt Nielsen
Second Reader

Philip A. Durkee
Chairman, Department of Meteorology

THIS PAGE INTENTIONALLY LEFT BLANK

ABSTRACT

The objective of this thesis is to investigate the vertical distribution of dust and its impact on the top of the atmosphere radiance and associated remotely sensed thermal variability in the midwave infrared wavelengths. Due to the inconsistent availability and coincidence of in-situ data with dust events, model data was used to identify the vertical dust regions. The Navy Aerosol Analysis and Prediction System global aerosol model was used to determine mass concentration and vertical extent of dust. Mass concentration was converted to extinction and individual dust events were analyzed to characterize the vertical distribution, extinction, and optical depth. The average height was defined for specific dust regions of Iraq and Korea. This value was used to determine the impact of the dust layer on the top of the atmosphere radiance and brightness temperature in the wavelengths of interest. Radiative transfer software was used to determine the top of the atmosphere radiance of the modeled dust atmosphere. Resultant brightness temperature was calculated to obtain the thermal characteristics of the dust layer and associated atmosphere. The vertical distribution of the dust layer was varied with fixed atmospheric components to gain insight into the resultant variation of radiance and subsequent brightness temperature to provide a set of possible values for a regionally specific dust event.

THIS PAGE INTENTIONALLY LEFT BLANK

TABLE OF CONTENTS

LIST OF FIGURES

THIS PAGE INTENTIONALLY LEFT BLANK

LIST OF TABLES

THIS PAGE INTENTIONALLY LEFT BLANK

ACKNOWLEDGMENTS

First, I would like to thank my advisor Dr. Philip A. Durkee. His Remote Sensing class inspired my choice of this topic and his patience, focus, and frequent course corrections kept me from straying from the final goal. I would also like to thank Mr. Kurt Nielsen for his guidance and input as second reader.

I would also like to express my appreciation to Dr. Jianglong Zhang and the Navy Research Lab Monterey for providing the data sets and expertise with the Navy global aerosol model. I would also like to thank Mr. Robert Creasey for technical assistance well beyond the call of duty. Without them, all of the data for this thesis would never have been analyzed. To my classmates who helped me through the entire process with their knowledge and great attitude, thank you and good luck in your future endeavors.

Finally, I would like to thank my loving wife for her unwavering love, confidence, and emotional support. Her focus and dedication to all aspects of life inspired me to attend graduate school and kept me motivated throughout the academic challenges.

THIS PAGE INTENTIONALLY LEFT BLANK

I. INTRODUCTION

The vertical variation of dust is a little-studied quantity. Until recently, in-situ measurement of the vertical distribution of dust has not been possible. With the advent of specialized instruments such as limb sounders and airborne and orbiting LIDAR technology, scientists are now able to directly measure the vertical region where dust occurs and model the behavior so accurate forecasts can be made. Dust is one of the most visible and common aerosols impacting the earth's radiation budget and our daily lives. Common to every inhabited continent, dust impacts areas where humans live and work and can therefore impact nearly every populated corner of the globe. Aerosolized dust has been studied by many scientists and researchers and yet, as its properties are becoming better understood, there is still much to learn. Arid and semi-arid regions of the world, which are the major potential source of dust, cover about a third of the earth's surface. Desert aerosol experiences the largest variability of all aerosol types by virtue of its physical and optical properties (D'Almeida *et al.,* 1991). The physical variability, specifically the variation with regard to height along with the radiative impact is the primary focus of this study.

As remote sensing technology becomes more advanced, understanding radiative transfer in the midwave infrared is emerging as a relatively new area of scientific concentration. As we begin to determine the components of the atmosphere which impact the midwave infrared, we can then ask how to compensate for those "unwanted" constituents in satellite measurements. In wavelengths shorter than 1 μm or longer than 8 μm, either reflected solar or emitted terrestrial radiation dominate respectively. The nebulous region of the midwave infrared is more complicated due to both solar and thermal sensitivities along with highly dynamic diurnal effects.

In the midwave infrared, the reflected solar irradiance combines with the emittance from the earth's surface along with the path emission to give the total top of the atmosphere radiance as measured by earth orbiting sensors. In these wavelenghs, both the solar term (reflected solar irradiance) and the thermal emittance term are significant contributors and are highly variable with wavelength.

Aerosol size, shape, and number distribution are critical in determining radiative impacts within specific wavelengths. In the midwave infrared, aerosols such as sulfate, smoke, sea salt, and dust have a profound impact on measured radiance through their complex reflective and absorptive/emissive properties. Because dust occurs as a result of dynamic meteorological processes, this study attempts to undertake the task of identifying the vertical variation of dust and how that variation affects the top of the atmosphere radiance in the 3-5 μm wavelengths. This study also provides insight to how this variation impacts the top of the atmosphere brightness temperature across the midwave infrared spectrum. Many other regions of the world exhibit significant dust storm events. For the sake of scale, military significance, and data collection, this study focuses on two source regions; one in southern Iraq, and the other is the Gobi Desert with dust impacts over the Korean Peninsula.

The goal of this study is to further our understanding of the radiative characteristics of the vertical variation of dust and to contribute to our ability to correct for atmospheric effects in the midwave infrared. Ultimately, once we can determine the impact of the intervening atmosphere, making calculations of upwelling radiance measured by satellite radiometers will allow more effective estimates of surface thermal characteristics. These estimates can be used in data assimilation to better improve forecast and climate models.

II. BACKGROUND

A. RADIATIVE TRANSFER AND THE MIDWAVE INFRARED SPECTRUM

Radiative transfer is the study of the essential energy flux in the atmosphere. It quantifies the transfer of energy between the sun, the earth and the atmosphere. In the case of no atmospheric absorption, the transfer is straightforward. Earth-bound or down-welling radiation from the sun is received at the earth as solar irradiance. The earth absorbs and reflects the solar radiation and emits radiation based on the surface temperature at the point of emission. When atmospheric effects are added, the radiative transfer problem becomes more complex. Depending on the wavelength and optical properties of the atmospheric constituents, some solar irradiance may be absorbed and/or reflected by the atmosphere. Additionally, some terrestrial radiation may be absorbed by the atmosphere.

The midwave IR is the region between the shortwave infrared (1-3 μm) and the longwave infrared (8-12 μm). It is a complex region in that there is not a continuously dominant radiation source across the spectrum. Figure 1 shows the Planck curves for both solar and terrestrial radiation assuming a 280 K surface. At 280 K, the wavelength where the solar and terrestrial radiation curves cross is roughly 4.7 μm. Using the Kidder and Vonder Haar's example of the surface as a 250 K blackbody, the solar radiation and terrestrial radiation are roughly equal at 5.7 μm. This demonstrates the variability of the crossing point as a function of the temperature of the earth's surface. As such, the midwave infrared represents a tremendously complicated and dynamic region for radiative transfer. That complexity makes radiative transfer in the midwave infrared challenging.

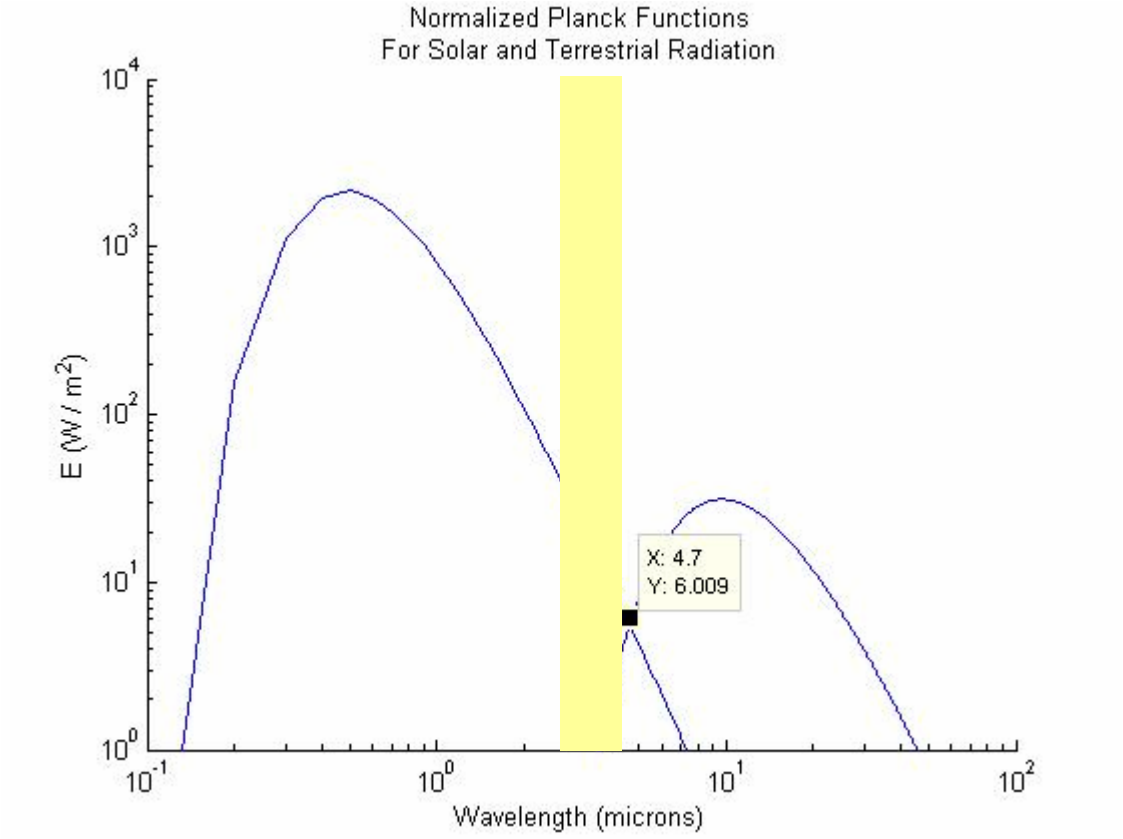

Figure 1. Planck Curves for Solar and Terrestrial Radiation Using 280 K Blackbody for the Earth Approximation.

Figure 1 shows Planck curves for solar irradiance and terrestrial exitance for a 280 K surface temperature. Solar radiation is the curve on the left peaking at roughly 0.48 µm and terrestrial radiation is the curve on the right peaking at roughly 10 µm. Notice the crossing point at 4.7 µm where values are nearly equal.

During daylight hours, the dominant photon source is highly wavelength-dependent with solar irradiance dominating up to approximately 4 µm and the terrestrial emission dominating at longer wavelengths. The midwave infrared is highly susceptible to the impacts of solar radiation and therefore depends on solar zenith angle, time of year, and the solar cycle. The nighttime radiance values depend on terrestrial emission with some reflected lunar impacts depending on the moon phase.

1. Solar Irradiance

Solar radiance as measured at the surface varies due to the distance from the sun to earth and the subsequent small angle subtended by the earth. Reflected solar radiation is a function of zenith angle and the surface albedo. Albedo is simply a ratio of reflected solar radiation to incident solar radiation. Since the path length of incoming solar radiation depends on the solar zenith angle, the radiation is scattered and absorbed along the path causing radiance depletion. Similarly, reflected solar radiation traveling through the atmosphere back to a sensor in low-earth orbit or geostationary orbit will also undergo depletion through scattering and absorption. Larger angles of incidence cause more depletion due to more scattering and absorption by greater amounts of intervening atmosphere.

2. Terrestrial Emittance

In contrast to reflected solar radiation, terrestrial emittance is only affected in one direction. As terrestrial radiation travels toward the orbiting sensor, energy is scattered and absorbed along the path causing depletion. Although the wavelength peak of terrestrial emission is near 10 μm, scattering and absorption by particles of size similar to the midwave infrared wavelengths have a large impact on radiative transfer within the terrestrial emission spectral band. Dust is one such particle type with size ranges from 0.01 μm to 100 μm.

3. Transmission Windows and Atmospheric Constituents Impacting the Midwave Infrared

Transmission of solar and terrestrial radiation through the atmosphere is impeded by normal atmospheric gaseous constituents such as water vapor, carbon dioxide, methane, and ozone. These constituents affect areas within the spectrum differently

causing degraded conditions at some wavelengths while allowing complete transmission at others. Figure 2 shows the transmittance across the midwave spectrum. There are several "window" bands with very little atmospheric impact.

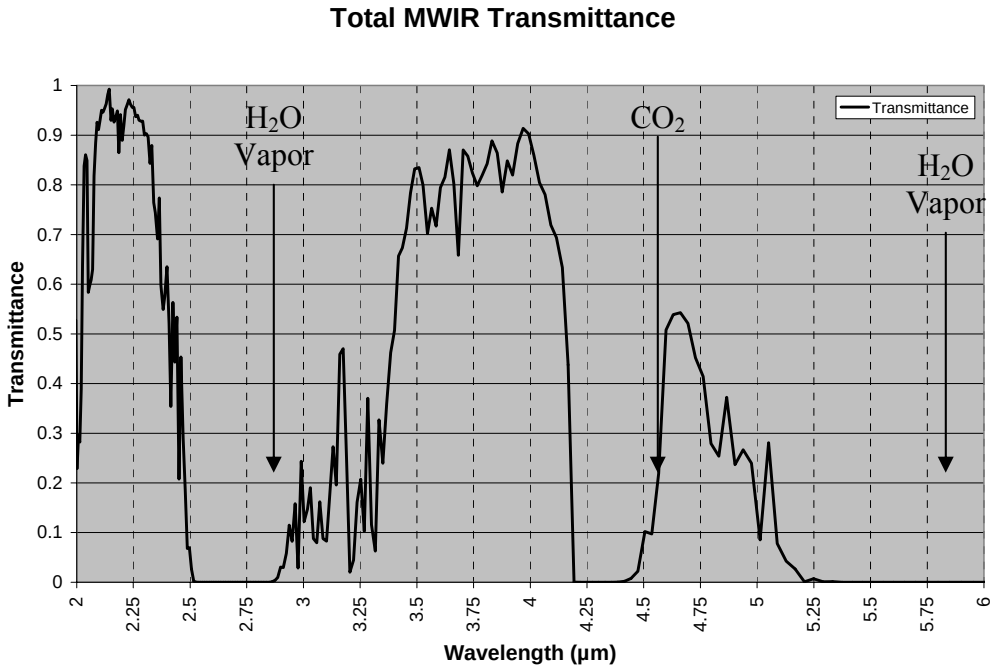

Figure 2. Transmittance in the Midwave Infrared

Kirchhoff's law of thermal radiation states that at thermal equilibrium, the emissivity of a body equals its absorptance (Kidder *et al.,* 1995). Thus, by Kirchhoff's Law of thermal radiation, a good absorber is a good emitter. Therefore the absorbing atmosphere also emits radiation at the ambient temperature of the atmosphere in which is resides. In the midwave infrared, there are several absorbing constituents. Table 1 shows absorption bands for water vapor (H_2O), Carbon monoxide (CO), Carbon dioxide (CO_2), and Methane (CH_4). The central absorption bands in the midwave infrared for the following gases are as follows: carbon dioxide absorbs at 2.69 µm, 2.76 µm, and 4.25 µm, carbon monoxide absorbs at 2.3 µm, and 4.7 µm, water vapor absorbs at 2.70 µm, 3.20 µm, and 6.30 µm and methane absorbs at 3.4 µm. The water vapor and carbon dioxide absorption bands are much broader in spectral scope while methane and carbon monoxide have much narrower bands.

Table 1. Molecular Absorption in The Midwave Infrared Spectrum (adapted from Ramanathan, 1978)

Absorption Bands of Atmospheric Gases	
Constituents	Absorption Bands (μm)
H_2O	0.5 - 2.0
H_2O, CO, and CO_2	2.0 - 3.0
H_2O and CH_4	3.0 - 4.0
CO and CO_2	4.0 - 5.0
H_2O	5.0 - 7.0

The midwave infrared "window" bands where there is relatively little absorption are from to 2.1 to 2.4 μm, 3.3 to 4.2 μm. Other bands may be used with careful consideration for molecular absorption. These bands are given for a dust free atmosphere in standard conditions using the 1976 US Standard Atmospheric components. When dust is added, optical depth increases resulting in a corresponding decrease in transmittance due to dust scattering and absorption.

B. TROPOSPHERIC DUST SOURCE REGIONS

1. China - Gobi Desert

Wind-blown dust originating from the arid deserts of Mongolia and China is a well known springtime meteorological phenomenon throughout East Asia. In fact, "yellow sand" meteorological conditions have acquired local names: Huangsha in China, Whangsa in Korea, and Kosa in Japan. The transport of desert dust from Asia to the North Pacific atmosphere is well documented and shows a maximum in dust loading each spring (Husar *et al.*, 1998). The overwhelming majority of Asian Dust storms occur in the spring as the polar jet retreats to the north and brings mid-latitude cyclones through northern Mongolia.

Figure 3. Main source region for Asian dust events including the Gobi Desert and Tibetan Plateau.

Source regions of Asian dust are located in east central and eastern Asia in the Gobi Desert and the northeast of the Tibetan Plateau. Figure 3 shows the dust source area of interest. Satellite measurements and climatological records make defining the dust source region for East Asia fairly straightforward. Desertification of the Gobi region along with the Tibetan Plateau has created a large source region centered in northern China and southern Mongolia. This region is virtually surrounded by mountain ranges particularly to the north and west. These mountains serve as the mechanism for significant surface wind in pre- and post-frontal dust scenarios.

As mid-latitude cyclones approach and pass through northern Mongolia, significant gap flows quickly accelerate surface winds in the Gobi region above 35 knots. Particle sizes can reach 100 μm in the immediate source region. Asian dust often travels thousands of kilometers and cases of Asian dust deposited in North America and Greenland are not uncommon. However, eastern China, the Korean Peninsula, and Japan are most impacted by these events.

2. Iraq - Dry Lake Beds and Alluvial Plains

Particularly fine silt and clay combined with the arid climate and unique geography make the Tigris-Euphrates alluvial plain the primary source for aerosolized dust in the region. Other point sources include dry lake beds to the northwest which are primarily composed of silt and clay. These point sources can cause significant dust events but are generally not of the geographical and temporal scope of the larger events caused by the primary source in southeastern Iraq.

According the UCAR COMET module on dust, the primary sources of dust in the Middle East are dry lake beds and the alluvial plain of the Tigris and Euphrates River plain (COMET MetEd, http://www.meted.ucar.edu/mesoprim/dust/, February 2007). This region is the primary source of aerosolized dust and is composed of silt and clay. In addition, the Syrian Desert and the Arabian Desert in Saudi Arabia contribute to dust events during large spring and autumn mid-latitude storms. These regions are composed of fine and coarse sand and, to a lesser degree, silt.

There are two primary meteorological causes of dust events in the Middle East. The first is the mid-latitude storm producing prefrontal and/or postfrontal dust events. The interaction between the polar jet and subtropical jet over the northern Arabian Peninsula in the spring and fall acts to enhance the horizontal and vertical motions resulting in significant aerial dust coverage as well as vertical transport. The second cause is the summer Shamal. This enhancement of the northern wind along the eastern half of Iraq bounded by the Zagros Mountains of Iran is the result of high pressure centered over the northern Arabian Peninsula, low pressure over central Iran, and the monsoon trough in the Indian Ocean. These interactions, combined with much warmer temperatures can loft dust above 5000 feet for days and sometimes weeks at a time.

Figure 4 identifies dust source regions for the Middle East. In Fig. 4a, high probability source regions are identified including the Tigris-Euphrates River plain (COMET MetEd, http://www.meted.ucar.edu/mesoprim/dust/, February 2007). In Fig. 4b, the climatological point sources are identified through the long-term study of satellite imagery using the US Air Force Defense Meteorological Satellite Program. These

sources are primarily dry lake beds with high silt and clay concentrations. In Fig. 4c, a true color Sea-WiFS image depicts summer Shamal lofting dust from central Iraq over the northern Persian Gulf. The highlighted circle depicts the source region for the aerosolized dust for the Iraq case study in the following chapters.

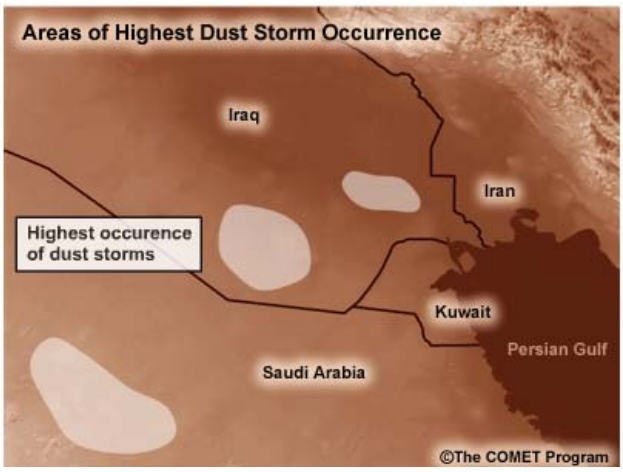

(a)

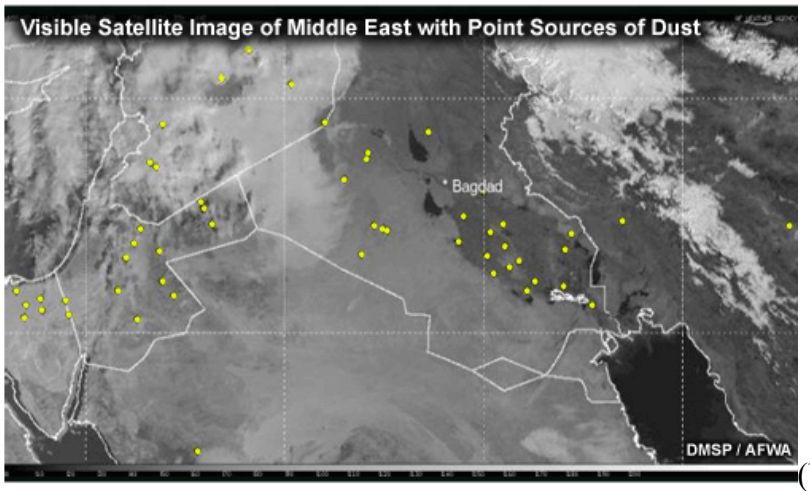

(b)

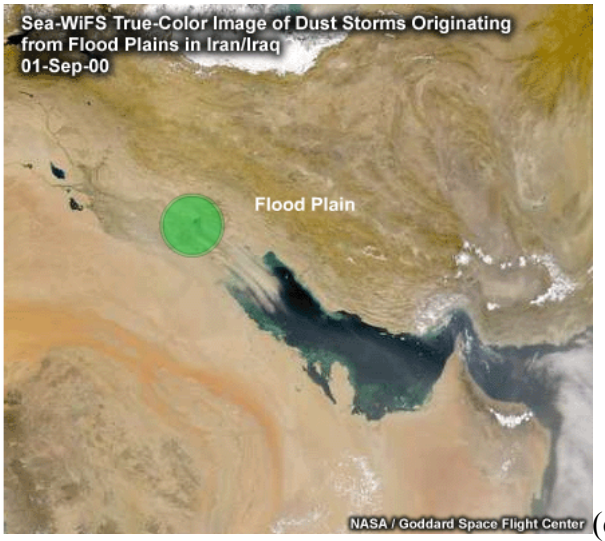

(c)

Figure 4. Dust Source Regions of Iraq and the Middle East (adapted from COMET MetEd, http://www.meted.ucar.edu/mesoprim/dust/, February 2007).

C. NAVY AEROSOL ANALYSIS AND PREDICTION SYSTEM (NAAPS)

1. Model Description

The Navy Aerosol Analysis and Prediction System (NAAPS) global aerosol model was derived from a modified form of that developed by Christensen (1997) and is run by the Naval Research Laboratory, Marine Meteorology Division, Monterey, CA, under the guidance of Dr. Doug Westphal. It uses global meteorological fields from the Navy Operational Global Atmospheric System (NOGAPS). The model is based upon the Optical Properties of Aerosol and Clouds (OPAC) defined by Hess *et al.,* (1998). NAAPS is run on a global 1 x 1 degree grid at six hour increments with 25 vertical levels based on the NOGAPS sigma levels up to 100mb. According to the NAAPS webpage, strengths of the model include the use of operational dynamics, 120 hour forecasts, near real time operation, global coverage, and dust and smoke simulations. Areas currently under further development are improvement of the dust source function, verification of sulfate simulations, and improvement of the microphysics and chemistry (Description of NAAPS, http://www.nrlmry.navy.mil/aerosol_web/Docs/globaer_model.html, February 2007).

NAAPS works on the premise that dust is lofted whenever the friction velocity exceeds a critical value, the snow depth is below a critical value, and surface moisture is below a critical value. In accordance with Westphal *et al.,* 1988, the flux is scaled to only include particles smaller than 5 μm and is allowed in the lowest two layers of the model. The friction velocity threshold is set for known dust emission areas in accordance with eight of the United States Geological Survey (USGS) land cover types. The Naval Research Laboratory, Marine Meteorology Division, Monterey, CA, has interpolated these eight USGS land use types to cover a 0.01 degree resolution and characterized the global land masses accordingly. The resolution was reduced to coincide with the NAAPS global aerosol 1x1 degree grid box.

The eight USGS land cover types which are identified in NAAPS as dust producing areas are: low sparse grassland, bare desert, sand desert, semi-desert shrubs, semi-desert sage, polar and alpine desert, salt playas, and sparse dunes and ridges.

The surface flux is scaled by the erodible fraction for each grid box and friction velocity is set to 0.6 m s^{-1} for all land types. The critical surface moisture is set to 0.3 and the critical snow depth value is set to 0.4 cm.

Table 2. Natural Aerosol Characteristics Source Strength, Atmospheric Burden and Optical Extinction Adapted from Ramanathan (2001)

Global source strength, atmospheric burden, and optical extinction due to the various types of aerosols (for the 1990s)					
Source	**Flux (Tg year $^{-1}$)**	**Lifetime (days)**	**Column Burden (mg m^{-2})**	**Specific scattering/ absorption (m^2/g)**	**Optical depth (×100) scattering/absorption**
Primary					
Dust(desert)	900-1500	4	19-33	0.6	1-2
Sea salt	2300	1	3	1.5	2
Biological debris	50	4	1	2	0.2
Secondary					
Sulfates from biogenic gases	70	5	2	8	1.6
Sulfates from volcanic SO_2 (troposphere)	20	10	1	8	0.8
Sulfates from Pinatubo (1991) (stratosphere)	(40)	(400)	(80)	(2)	(16)
Organic matter from biogenic hydrocarbons	20	5	0.6	8	0.5
Total natural	2400-3000		32-45		6-7 (±3)

From Table 2, it is clear that desert dust is responsible for roughly 1/3 of the total optical depth (excluding volcanic ash) based on global source strength measured during a 1990's study undertaken by Ramanathan *et al.,* (2001). It is second only to sea salt in global annual flux and the 4 day lifespan gives it a highly variable longer life than sea salt. In the case of Asian dust storms, particles with mass between 2.5 and 10 μg m^{-3} were found to increase four to six times over the background levels (Yuan *et al.,* 2004). This natural variability of the dust is the impetus for this study.

D. OPTICAL PROPERTIES OF AEROSOL AND CLOUDS (OPAC)

The software package Optical Properties of Aerosol and Clouds was developed by Hess *et al.,* (1998) to effectively manage the optical properties of aerosols within the solar and terrestrial spectral range. The variability of aerosols in number density, size distribution, shape, and height makes determining the point-in-time state quite difficult. The OPAC software package attempts to reduce this complexity without neglecting the likely variations in order to model the aerosol. In OPAC, this goal is achieved by the use of a dataset of typical clouds and internally mixed aerosol components (Hess *et al.,* 1998). Specifically, the NAAPS dust mass concentration incorporates the OPAC desert model for size, shape and number densities as well as optical properties. Desert aerosol size distribution tends to exhibit three overlapping modes at diameters of 0.01 μm or less, 0.05 μm, and 10 μm (Seinfeld 1998). The OPAC desert model components are listed in Table 3 and the size distribution is shown in Fig. 5.

Table 3. OPAC Software Package Composition of Desert Aerosols for 50% Relative Humidity

Component	**N_i (cm^{-3})**	**M_i ($\mu g\ m^{-3}$)**	**Number Mixing Ratios (n_j)**	**Mass Mixing Ratios (m_j)**
Mineral (coa.)	0.142	45.6	0.617E-4	0.202
Mineral (acc.)	30.5	168.7	0.133E-1	0.747
Mineral (nuc.)	269.5	7.5	0.117	0.033
Water Soluble	2000	4.0	0.87	0.018
Total	2300	225.8	-	-

OPAC assumes a spherical shaped dust particle with log-normal size distributions consisting of a mixture of quartz and clay minerals modeled with three distinct modes to capture the increasing relative amount of larger particles for increasing turbidity and mie scattering theory is used in calculation the optical properties (Hess *et al.,* 1998). The accumulation mode is the primary contributor to the mass concentration with a mass mixing ratio of 0.747. Figure 5 shows the size distribution for particle radii of 0.01 to 10 μm range.

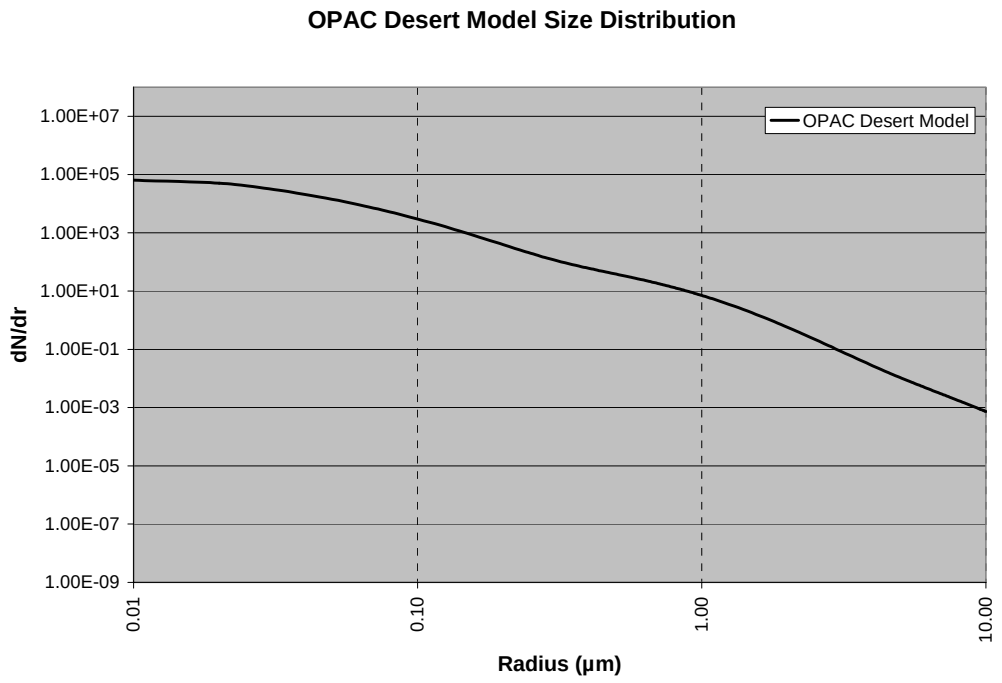

Figure 5. OPAC Desert Model Size Distribution

E. MODERATE RESOLUTION ATMOSPHERIC TRANSMISSION (MODTRAN) RADIATIVE TRANSFER MODELING SOFTWARE

This study used the MODTRAN 4 software for the computation of all radiance and transmittance values. MODTRAN is modeling software created by the Air Force Research Laboratory used for computing radiative properties including radiance and transmittance for frequencies from 0 to 50,000 cm^{-1} at 2 cm^{-1} spectral resolution. It incorporates spherical and refractive geometry, solar and lunar source functions for both

Rayleigh and Mie scattering, and allows multiple scattering and multiple viewing angles. Recent improvements to MODTRAN allow multiple scattering using a Bi-directional Reflectance Distribution Function (BRDF) which gives the reflectance of a target as a function of illumination geometry and viewing geometry. This allows scattering to be other than Lambertian, producing more accurate results (MODTAN 4 Software, http://www.vs.afrl.af.mil/ProductLines/IR-Clutter/modtran4.aspx, February 2007).

1. MODTRAN Input Parameters

Using the OPAC Software Package and the desert model values listed in Table 3, the scattering phase function, extinction coefficient, absorption coefficient, single scatter albedo, and asymmetry parameter for the desert model were calculated at 3, 4 and 5 μm wavelengths. MODTRAN input cards with vertical atmospheric profiles and layer extinction values calculated from mass concentration from NAAPS were created and added to the spectral optical values. Tables 4 and 5 list these values normalized to 0.55 μm (as required by MODTRAN).

In this study, standard values for atmospheric gases were used. The default values for CO, CO2, H2O, O3, N2O, CH4 and MODTRAN defined heavy species were used corresponding to mid-latitude winter defaults for the Korean Peninsula dust scenario and mid-latitude summer for the Iraq dust scenario. Caution should be used in interpreting the absorption bands for each of these constituents as present atmospheric values have changed for each of these quantities.

Table 4. MODTRAN Spectral Input Parameters

wavelength (μm)	**ext. coef. (1/km)**	**abs. coef. (1/km)**	**asymmetry parameter**
3	0.67464	0.14960	0.7154
4	0.51965	0.15110	0.6774
5	0.40480	0.15200	0.6182

The OPAC derived scattering phase functions normalized to 0.55 μm for each wavelength can be found in Table 5 below.

Table 5. MODTRAN User Input Scattering Phase Functions

	Wavelength (μm)		
θ	3	4	5
0	60.568	37.157	24.216
2	40.342	28.682	20.116
4	26.065	20.208	14.808
6	19.292	15.485	11.455
8	15.480	12.644	9.298
10	12.983	10.741	7.825
12	11.149	9.344	6.749
16	8.511	7.342	5.237
20	6.633	5.890	4.177
24	5.211	4.755	3.372
28	4.118	3.849	2.733
32	3.267	3.117	2.220
36	2.605	2.526	1.807
40	2.087	2.054	1.473
52	1.107	1.122	0.812
60	0.749	0.767	0.557
68	0.523	0.538	0.391
80	0.323	0.334	0.242
92	0.218	0.226	0.163
100	0.177	0.184	0.132
108	0.150	0.157	0.113
120	0.129	0.138	0.098
124	0.126	0.136	0.096
132	0.125	0.139	0.096
136	0.126	0.143	0.098
140	0.129	0.150	0.102
146	0.134	0.165	0.109
150	0.137	0.179	0.115
156	0.141	0.204	0.126
160	0.140	0.221	0.133
166	0.139	0.234	0.134
170	0.147	0.245	0.134
176	0.175	0.288	0.149
180	0.186	0.314	0.159

The OPAC-derived scattering phase functions for each wavelength were used up to 100 mb and the default MODTRAN phase functions were used for the remainder of the column. Multiple scattering with four streams was selected as the default scattering mechanism to create the MODTRAN output values for radiance and transmittance. All MODTRAN runs were calculated based on a nadir low-earth orbit viewing angle and altitude.

F. EXTINCTION, OPTICAL DEPTH, AND BRIGHTNESS TEMPERATURE

In order to determine the vertical variation of dust and how it impacts satellite measured radiance, we must know the character of the dust. From the NAAPS and OPAC data, extinction and subsequent optical depth can be calculated using the NAAPS aerosol mass to optical depth transfer function. Brightness temperature is calculated from radiance output from radiative transfer modeling software.

1. Extinction

The standard form of volume extinction coefficient is calculated as the sum of the scattering and extinction coefficients

$$\sigma_e = \sigma_a + \sigma_s \tag{1}$$

where the absorption coefficient is

$$\sigma_a = C_{mi} * \alpha_{ei} * (1 - \omega_o) \tag{2}$$

and the scattering coefficient is

$$\sigma_s = C_{mi} * \alpha_{ei} * \omega_o \tag{3}$$

In this form, C is the volume dust mass concentration in (g m^{-3}), scaled by the dry dust mass extinction efficiency α in (m^2 g^{-1}). The single scatter albedo ω_o is used to separate the scattering and absorption components.

2. Optical Depth

For Aerosol optical depth δ, Kidder and Vonder Haar define the vertical optical depth as the vertically integrated volume extinction as follows

$$\delta(z_1, z_2) = \int_{z1}^{z2} \sigma_e(\lambda, z)\, dz \tag{4}$$

Because there are 25 layers in the NAAPS model, an approximation for aerosol optical depth is used and is defined as the vertical sum of each volume extinction value from the NAAPS mass concentration. This is accomplished by using the aerosol mass to optical depth transfer function

$$\delta_\lambda = \sum_i \alpha_{ei}(\lambda) * C_{mi} * f_{ei}(RH, \lambda) \tag{5}$$

where δ is the aerosol optical depth calculated by the vertical sum of the model layer mass concentration C (g m-3) scaled by the mass extinction efficiency, α (m2 g-1), multiplied by the aerosol hygroscopic growth factor for extinction, f. The mass extinction cross-sections (as a function of wavelength) for dust are obtained from OPAC (Hess *et al.*, 1998) and can be found in Table 4. Assuming dust is hydrophobic, the aerosol hygroscopic growth factor is one. Optical depth values given in this study are normalized to 0.55 μm for consistency.

3. Brightness Temperature

Calculating brightness temperature from spectral radiance requires the use of Planck's Law of Blackbody Radiation. In standard form the equation is

$$L_\lambda = \frac{2hc^2\lambda^{-5}}{e^{\frac{hc}{\lambda kT}} - 1} \tag{6}$$

where

L(λ, T) is the wavelength and surface temperature dependent radiance,

h = Planck's Constant (6.626068 E -34 J s),

k = Boltzman's Constant (1.38066 E -23 J deg^{-1}),

c = the speed of light in a vacuum (2.997925 E 8 m s^{-1}), and

T = surface temperature in Kelvin

From Smith (2005), calculating brightness temperature can be accomplished by first inverting the Planck Function

$$e^{\frac{hc}{\lambda kT}} - 1 = \frac{2hc^2\lambda^{-5}}{L_\lambda} \tag{7}$$

and taking the natural log for both sides

$$\frac{hc}{\lambda kT} = \ln\left[\frac{(2hc^2\lambda^{-5})}{L_\lambda} + 1\right] \tag{8}$$

after isolating temperature,

$$\mathrm{T} = \left(\frac{hc}{k\lambda}\right)\left(\frac{1}{\ln\left[\frac{(2hc^2\lambda^{-5})}{L_\lambda} + 1\right]}\right) \tag{9}$$

we can make the substitutions

$$K_1 = 2hc^2\lambda^{-5} \qquad K_2 = \frac{hc}{k\lambda} \tag{10}$$

and the formula for brightness temperature from radiance becomes:

$$T = \frac{K_2}{\ln\left(\frac{K_1}{L_\lambda} + 1\right)} \tag{11}$$

Once the wavelength-dependent radiance values were calculated by MODTRAN, the data were imported into spreadsheet software which was used to accomplish the brightness temperature calculation and graphing for further analysis.

THIS PAGE INTENTIONALLY LEFT BLANK

III. DATA

A. NAVY AEROSOL ANALYSIS AND PREDICTION SYSTEM OUTPUT

The NAAPS data sets included global grid fields for March through May 2001 and 2002 as well as selected dates from 2002 through 2006. The data included latitude, longitude, model level, mid layer pressure, layer thickness, mid-layer temperature, mass concentration for dust, mass concentration for smoke and mass concentration for sea salt.

The data sets were defined for the dust events of study based on duration, aerial coverage, vertical extent, verifying satellite imagery, and location of the affected area of the dust event. Two cases were chosen for the study, one in central North Korea from March 20-23, 2002 and one in Southern Iraq from May 13-15.

The ASCII data files for each event covered the corresponding 6 hourly NOGAPS data set giving a total of four files per day. Each file was formatted using IDL to calculate height AGL from thickness, re-orient arrays for use by other software, and subset the data to the specific area of interest. The IDL output was given in unformatted binary code for ingest into three dimensional visualization and simulation software.

B. VIS5D VISUALIZATION AND SIMULATION SOFTWARE

Vis5D is a system for interactive visualization of large 5-D gridded or binary data sets such as those produced by numerical weather models (Vis5D, http://www.ssec.wisc.edu/~billh/vis5d.html , February 2007). Once the data are ingested, they can be manipulated in x, y, and z directions to create varying perspectives, isosurfaces, vertical and horizontal cross sections, and volume renderings of any or all of four possible user-defined variables within a 3-D space rendering. The data can be depicted over three dimensional topographical maps and rotated and animated in real time. Vis5D is open source software available through University of Wisconsin to

anyone with a Unix/Linux capable computing platform. Figure 6 represents dust mass concentration renderings within Vis5D for each case during the peak optical depth produced.

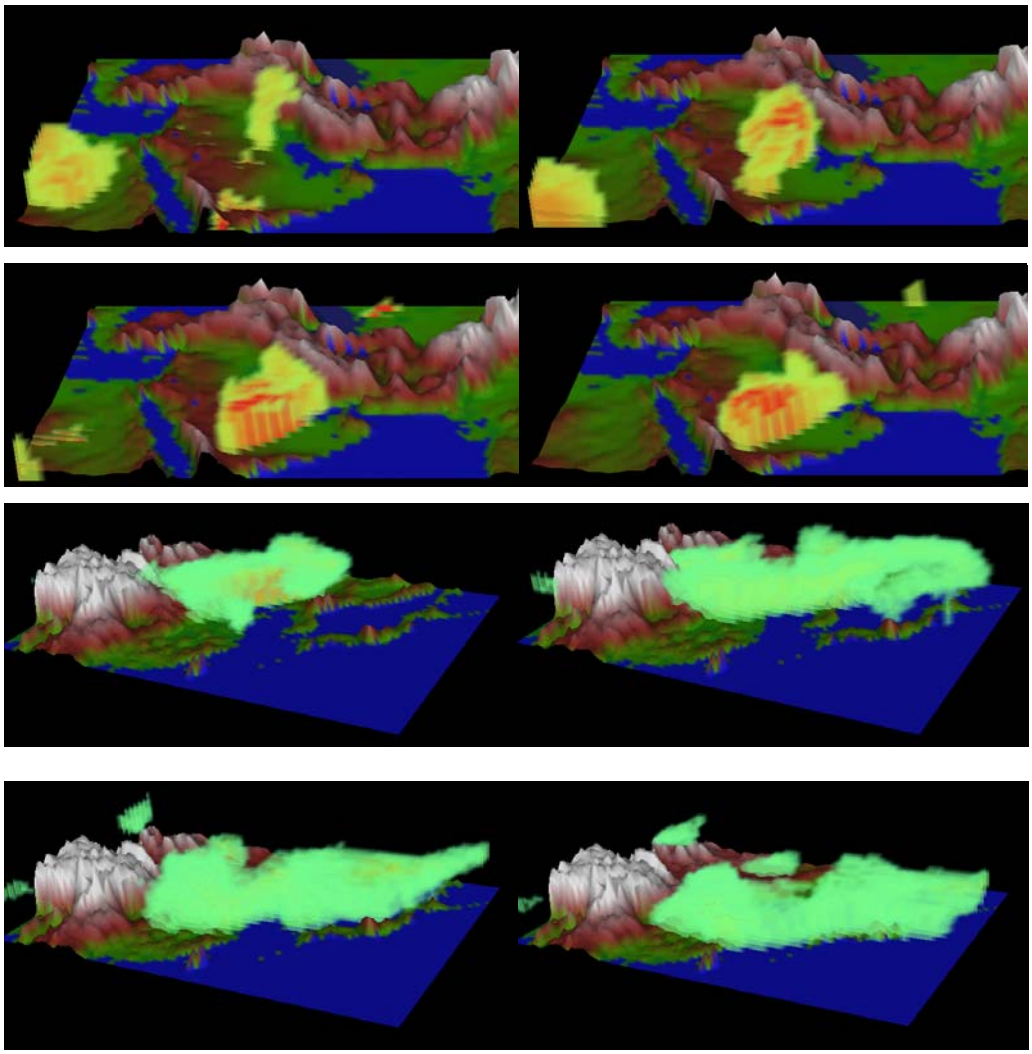

Figure 6. Vis5D Depiction of High AOD Dust Over The Middle East (top 4 panels) and East-Asia (bottom 4 panels)

C. MODERATE RESOLUTION IMAGING SPECTRORADIOMETER (MODIS)

The MODIS instrument suite consists of components aboard two satellites from the Earth Observing System called Aqua and Terra. Both are sun-synchronous polar

orbiting satellites with near circular orbits at 98.2 degree inclination orbiting at approximately 705 km. Terra is "morning" satellite with a descending node crossing the equator at 10:30 AM local and Aqua is the "afternoon" satellite with an ascending node crossing the equator at 1:30 PM local. A ±55-degree scanning pattern achieves a 2,330 Km swath offering the capability of total earth coverage every 24-48 hours (NASA Goddard Space Flight Center, 2007).

The MODIS instrument is a scan mirror assembly which operates at 12 bit sensitivity in 36 spectral bands ranging from visible (0.405 μm) to thermal infrared (14.385 μm). MODIS has a 6 year design life and Terra, launched in 1999, has already outlived its design.

The MODIS data are provided in HDF format are delivered by file transfer protocol. The software suite ENVI was used to view the files.

D. MODTRAN OUTPUT

MODTRAN output files are generated after the user input file has been run through the radiative transfer algorithm. They are in ASCII format readable with any text file reading program. The file repeats the user input followed by the spectral output data including path thermal emission, solar irradiance, path scattered radiance, ground reflected radiance, total radiance, and total transmittance.

THIS PAGE INTENTIONALLY LEFT BLANK

IV. METHODS AND PROCEDURES

This chapter outlines the methods and procedures undertaken in the selection of areas of interest, calculation of extinction and optical depth for each time step, radiance, transmittance calculations, and brightness temperature calculations for both the actual cases and the idealized atmospheric and dust cases.

A. ESTABLISHING AREAS OF INTEREST AND CASE STUDIES

Satellite imagery and model output were used in order to determine the fixed points of interest. MODIS imagery was used to identify times and areas of dust events and validate the mass concentration values given by NAAPS. Vis5D was used to create three dimensional volume renderings, cross sections, and time series simulations for dust mass concentration, layer temperature, height above ground and layer thickness.

1. Gobi Desert Dust Event

Climatologically the majority of dust events over the Korean Peninsula occur in the spring between the months of March and May. A visual inspection of MODIS RGB composite satellite imagery allowed dust detection for multiple dates during the Aerosol Characterization Experiment-Asia timeframe. Longer duration events were favored in order to obtain multiple days of dust over the point of interest.

After careful evaluation, the dust event over North Korea from March 20-25, 2002 was selected due to consistently dusty imagery. Figure 7 depicts the storm with (a) showing the dust storm inception on March 19, 2002 as the result of wind channeling through mountain passes due to a mid-latitude cyclone in northern Mongolia and (b) showing the advected dust or "Yellow Sand" over the Korean Peninsula and extending out to northern Japan under cloud cover on March 20, 2002. This storm continued to blow significant dust over the Korean Peninsula through March 23, 2002. The point at 39.0° north latitude and 126.0° east longitude was chosen to represent North Korea.

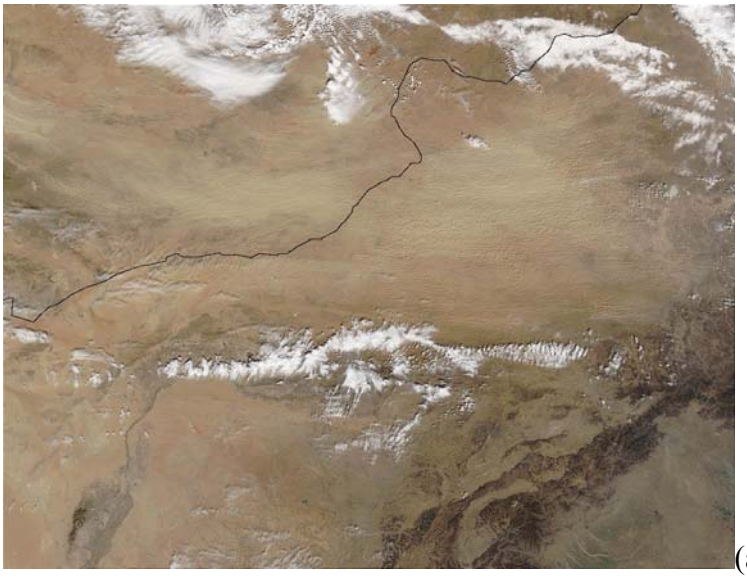

(a)

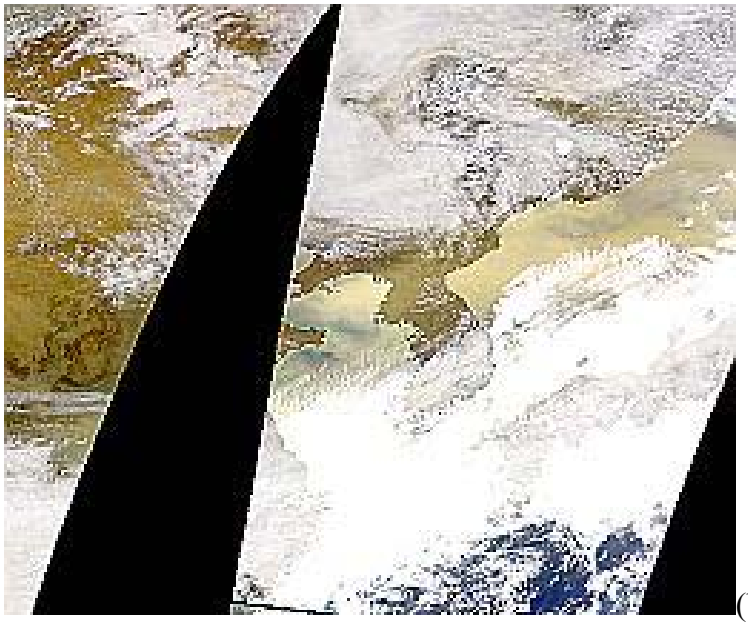

(b)

Figure 7. Gobi Dust Storm and Resultant Dust Plume Over The Korean Peninsula

Some cloud masking is visible over the dust layers in North and South Korea and throughout Japan. Since this study uses modeled data, cloud masking is not a factor in determining aerosol optical depth or vertical dust distribution.

2. Iraq Dust Event

The method for finding a suitable dust event for the Iraq case study was similar to the method used for the Korean Peninsula case. MODIS composite RGB satellite imagery from known dust events was analyzed to find a suitable case with sufficient spatial and temporal size. The point 31.0° north and 47.0° east was chosen to represent Iraq.

Figure 8. Southern Iraq and Persian Gulf Dust Event

The dust event in southern Iraq was the result of a summer Shamal which created a large dust plume which rotated around high pressure in western Iraq. In addition, previous storm activity in the Nile River Valley increased ambient aerosolized dust over Iraq prior to this event.

B. EXTINCTION, OPTICAL DEPTH, RADIANCE, AND TRANSMITTANCE

1. Extinction

Extinction was calculated using the bulk method outlined in Chapter II section F. The mass concentration for each volume cell extending vertically over the points of interest was multiplied by the volume extinction coefficient to calculate the mass extinction per meter for the layer. The layer extinction was multiplied by the thickness in meters of the layer to calculate the layer extinction.

2. Optical Depth

Because optical depth is the vertical integral of extinction, an approximation for optical depth was calculated by using the sum total of all 25 layer extinction values. High and low ranges were based on the largest modeled optical depth and the smallest modeled optical depth. Optical depth values given in this study are normalized to 0.55 μm for consistency.

3. Radiance and Transmittance

Radiance and transmittance were calculated based on the user inputs into MODTRAN. After formatting the user-defined atmosphere including the pressure, temperature, height, and extinction for each layer at each 6 hour time step, the MODTRAN radiative transfer software output radiance and transmittance in text file format.

C. IDEALIZED CASES FOR THE IRAQI DESERT AND KOREAN PENINSULA

After determining the vertical extinction for each time step of each case, the averages were calculated for the extinction and vertical atmospheric values to create a pseudo-standard dust atmosphere. For temperature, pressure, and thickness, the average was used to create a standard for each case. The heavy to light range for optical depth was used to create three aerosol optical depth bins according to the maximum and minimum dust aerosol optical depth observed in the case studies. The vertical variation was determined by observing the extinction vs. height curves for each time step of the dust event. The high to low range for the dust altitude was used to create three height bins according to the highest and lowest altitude of 50% of the maximum extinction.

The average atmosphere was set as the static setting in MODTRAN while the aerosol extinction and height values were varied to create 10 separate extinction profiles for each case including; light-low, medium-low, heavy-low, light-mid, medium mid, heavy-mid, light-high, medium-high, heavy-high, and no dust. The radiance and transmittance values were calculated for each profile through MODTRAN for both a day scenario and a night scenario.

The MODTRAN radiance and transmittance were graphed for examination and further calculation. The brightness temperature from each radiance value at each wavelength was also calculated in order to compare the effect of varying the height and mass optical depth on satellite received temperature values.

THIS PAGE INTENTIONALLY LEFT BLANK

V. RESULTS

The results of this study are broken into two sections. First, the case studies for North Korea and Iraq which determine the baseline values for dust in their respective regions. Second, the idealized dust scenarios over fixed atmospheres representing each of the regions in the case studies are described.

A. CASE STUDIES

1. Korean Peninsula

The Korean Peninsula case study is based on a dust event which began in the Gobi Desert on March 18, 2002. The storm lasted through March 23, 2002. The dust effects were modeled over North Korea at 39.0° north latitude and 126.0° east from March 20, 2002 through March 23, 2002.

a. Extinction Due to Dust

For the first study, the results of the vertical extent of the dust were somewhat surprising. The dust extended to a much greater altitude than expected. On March 21st at 1800 UTC the greatest concentration of dust was observed at 4.5 km with the extinction value reaching 0.16 m^{-1}. The total optical depth for this time frame of 1.64 was the greatest seen for this case. The lightest optical depth of 0.14 occurred when there was no observable dust on March 23rd at 1200 UTC. The first day/time step where dust was observed was on March 21st at 0000 UTC with an optical depth of 0.47. This was the lightest optical depth observed in conjunction with the dust event over North Korea.

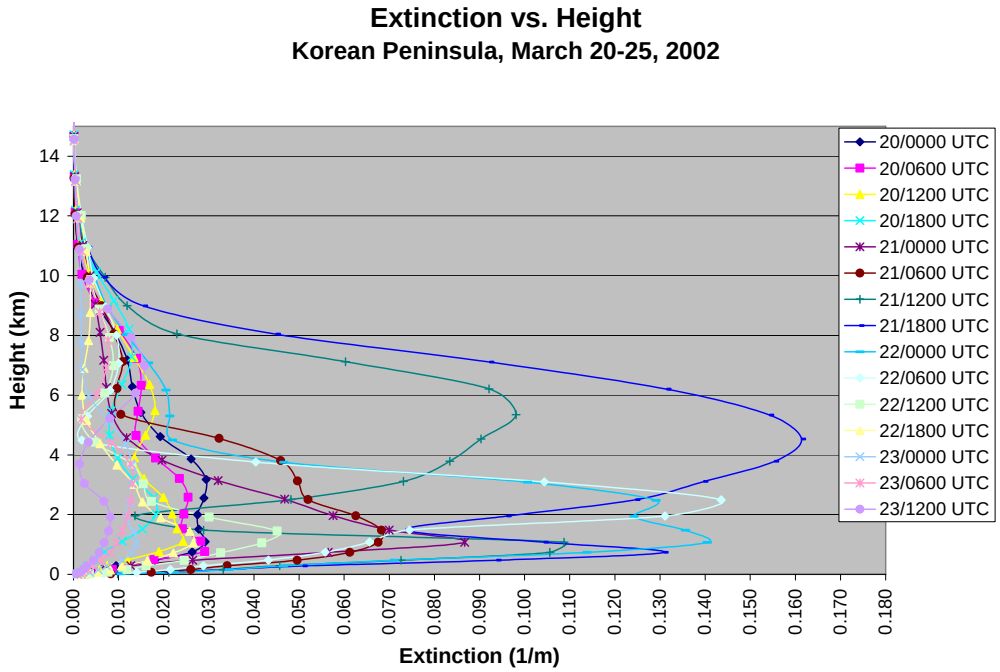

Figure 9. NAAPS Modeled Extinction vs. Height - Korea Case Study.

Figure 9 depicts the extinction values for each of the 15 time steps of the study. Note the vertical variability of the extinction peaks ranging from 1 to 5 km and the greater extinction values observed on March 21st at 1200 and 1800 UTC extending to 7 km. All time steps on March 20th along with March 23rd were considered non-event extinction values representing the normal background mass concentration for the area of interest.

b. Transmittance

Transmittance values for this study ranged from zero in the water vapor and carbon-dioxide absorbing bands centered at 2.7 and 4.3 μm respectively to 0.92 at 2.1 μm. This is a function of molecular absorption, the dust optical depth, MODTRAN input parameters, and the internal MODTRAN transmittance algorithm. In this case, the

MODTRAN input parameters for molecular models were based on mid-latitude winter gaseous constituents. The OPAC model generated optical properties were based on 50% relative humidity representing Korean atmospheric conditions in March.

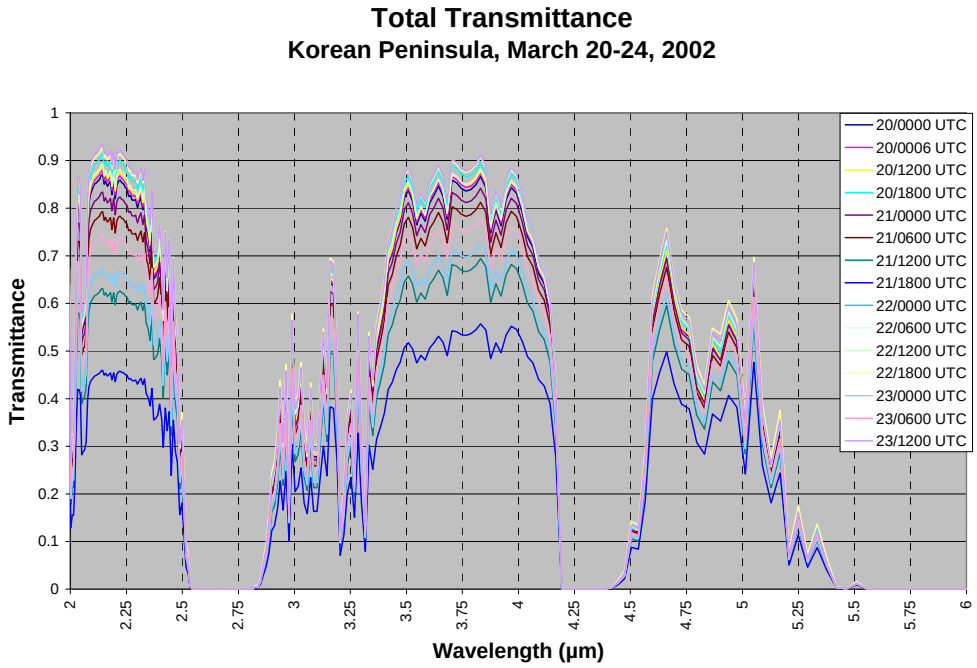

Figure 10. Transmittance - Korean Peninsula Case Study

The radiance values calculated for each day/time step and are shown in Fig. 11. A "No Dust Day" value is also plotted with all MODTRAN aerosol extinction values set to zero. The solar zenith angle plays a large part in the total reflected radiance and the difference between 0000 UTC and 0600 UTC can clearly be seen at wavelengths from 2 to 2.6 µm (shorter than the 2.7 µm water vapor absorption band).

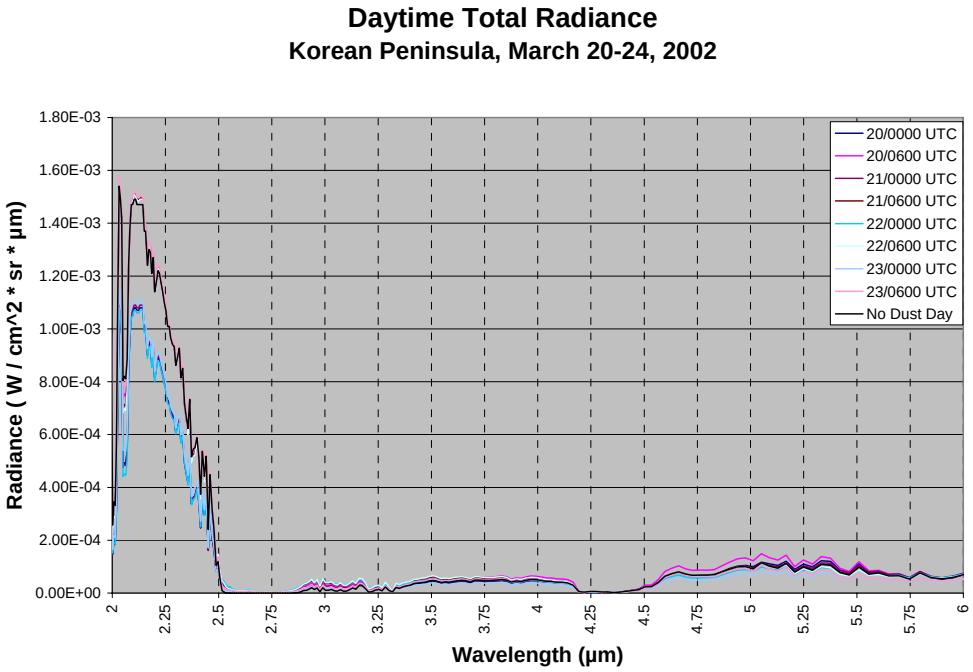

Figure 11. Korean Peninsula Total Daytime Radiance

The variation of the daytime radiance in the 3-5 µm band is relatively small. The largest difference for 3 µm occurs between March 22nd at 0600Z and the No Dust case with a difference of 4.60 x 10^{-5} W m^{-2} sr^{-1} μm^{-1}. While the numbers are small, the smallest value is 9.3 % smaller than the greatest. The radiance difference translates to a brightness temperature difference of 13.4 K. At 4 µm, the smallest value seen on the 22nd at 0600 UTC is 56.5% smaller than the greatest seen on the 23rd at 0000 UTC resulting in a brightness temperature difference of 4.6 K. At 5 µm, the smallest produced value seen on the 23rd at 0000 UTC is 55% smaller than the greatest value seen on the 20th at 0600 UTC resulting in a brightness temperature difference of 6.1 K.

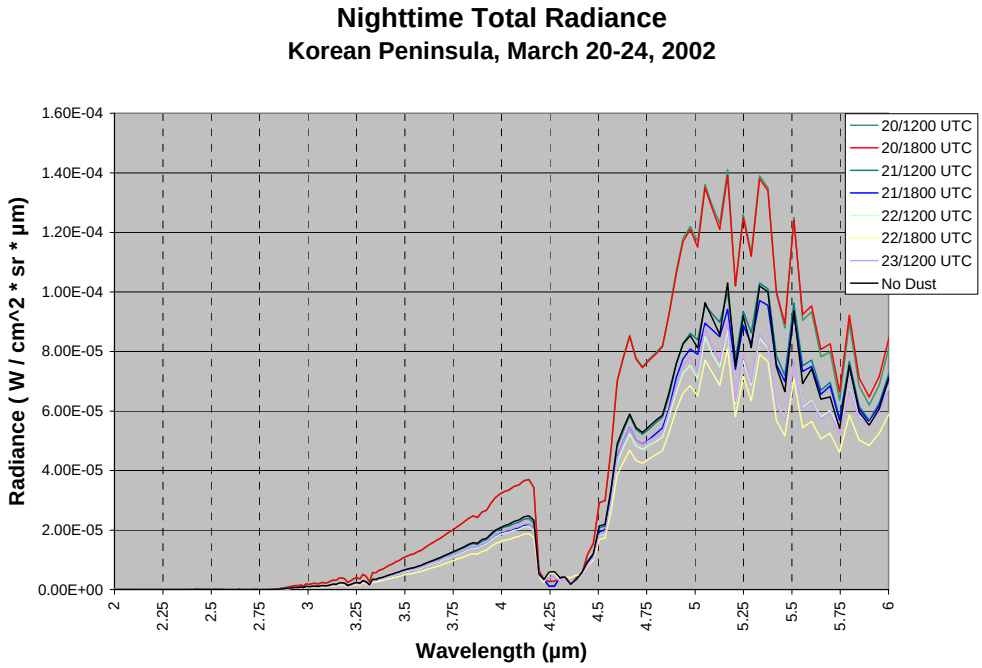

Figure 12. Korean Peninsula Total Nighttime Radiance

For the radiance during the night time steps shown in Fig. 12, the solar component is completely absent and the only available radiance is due to the surface and path terms. Of note here are the much larger modeled values on March 20th at 1800 UTC. This time step had the second warmest surface and average column temperature modeled. Higher temperatures combined with optical depth of 0.17 allowed more terrestrial radiation to reach the sensor.

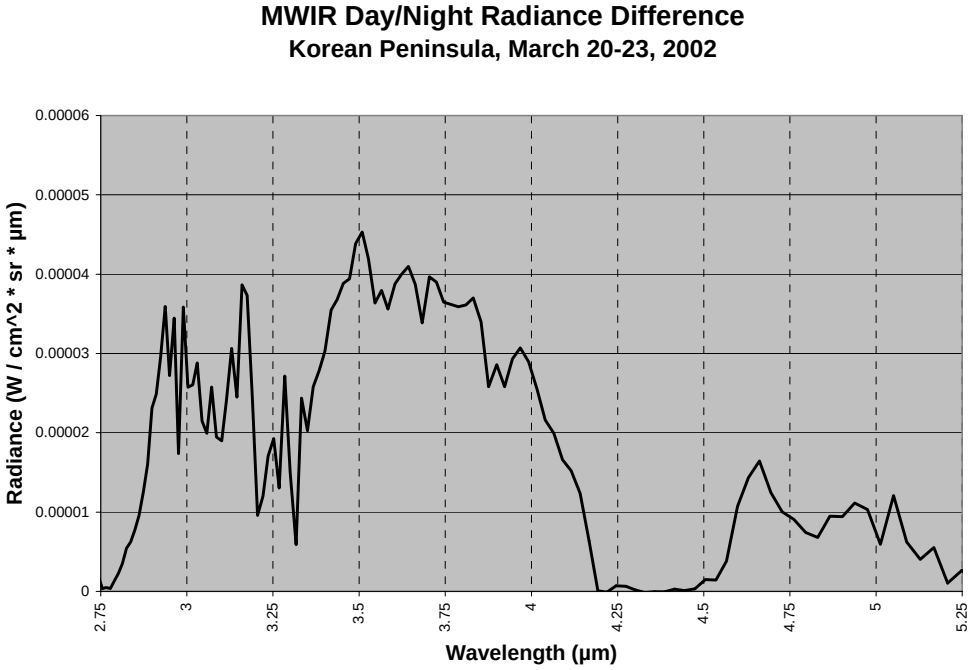

Figure 13. Average Day-Night Radiance Difference - North Korea Case

Figure 13 shows the difference between the day and night radiance values in the North Korea case study. The average solar contribution in the midwave bands was calculated as the difference between the daytime nighttime radiances. The greatest day/night radiance difference occurred at 3.509 µm with the average daytime radiance representing an 86% increase over the average nighttime radiance values.

It is important to consider that the difference in radiance values here are not simply the result of the variable height and mass concentration of the overlying dust. These cases are time steps within the NAAPS model run thus, not only is the dust mass concentration changing, but the atmosphere is changing as well. Temperature, pressure and layer thickness profiles change with each successive modeled time step. Therefore, we can not attribute the resultant radiance variance to dust alone.

2. Iraqi Desert

The Iraq desert case study is based on a dust event which began in the Tigris-Euphrates Alluvial Plain on May 13, 2004. The storm lasted through May 15, 2004. The dust effects were modeled over Southern Iraq at 31.0° north and 47.0° east.

a. Extinction Due to Dust

For the second study, the results of the vertical extent of the dust were not as surprising given the proximity to the source region and typical atmospheric heating in the summer months of Iraq. On May 15th at 1200 UTC the greatest concentration of dust was observed at 3.5 km. The total 0.55 μm optical depth of 1.45 was the greatest seen for this case. The lightest optical depth of 0.43 occurred when there was no observable dust on May 13th at 0000 UTC. The first time step where dust was advected over the area was on May 13th at 0600 UTC with a total optical depth of 0.81. The extinction curves for this event were generally restricted to lower altitudes but were more concentrated than the Korean event. This is due to the geographically closer proximity of the point selected to the source region.

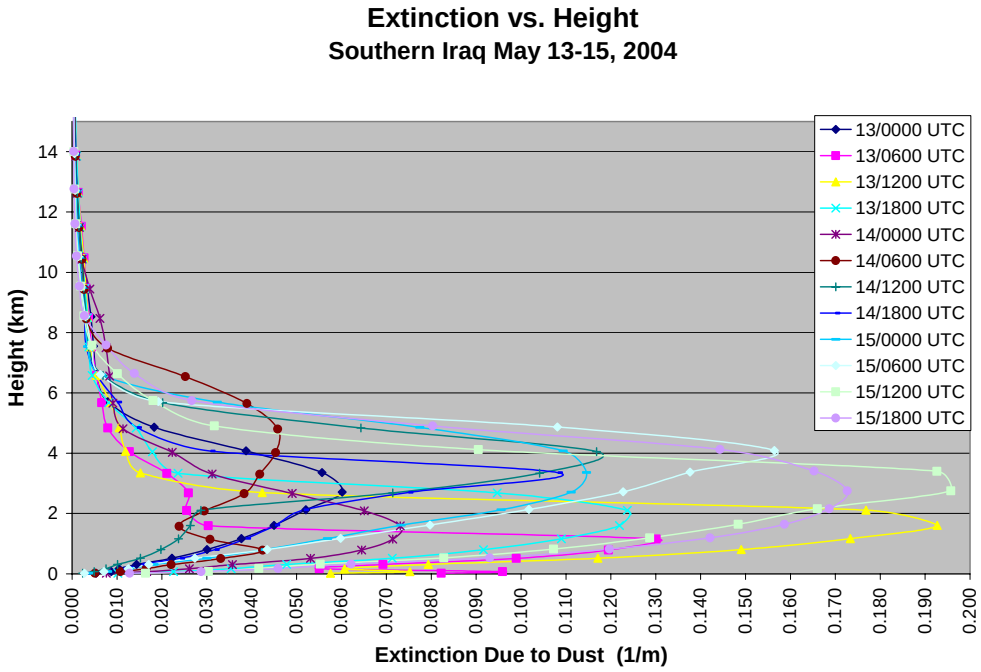

Figure 14. NAAPS Modeled Extinction vs. Height - Iraq Case Study.

Figure 14 depicts the extinction values for each of the 12 day/time steps of this study. Note the vertical variability of the extinction peaks ranging from 1 to 4 km with the greater extinction values observed on May 15th extending to 5 km. All time steps on May 14th were considered non-event extinction values representing the normal background mass concentration for the area of interest.

b. Transmittance

Transmittance values for this study ranged from zero in the water vapor and carbon-dioxide absorbing bands centered at 2.7 and 4.3 µm respectively to 0.83 at 2.1 µm. Again, this is a function of molecular absorption, the dust optical depth, MODTRAN input, and the internal MODTRAN transmittance algorithm. In the Iraq case, the input parameters for molecular models were based on mid-latitude summer molecular and atmospheric constituents along with a 0% relative humidity OPAC model

and desert albedo. The transmittance is less throughout the midwave spectrum in Iraq due to the greater background dust levels and subsequent greater optical depth in the region.

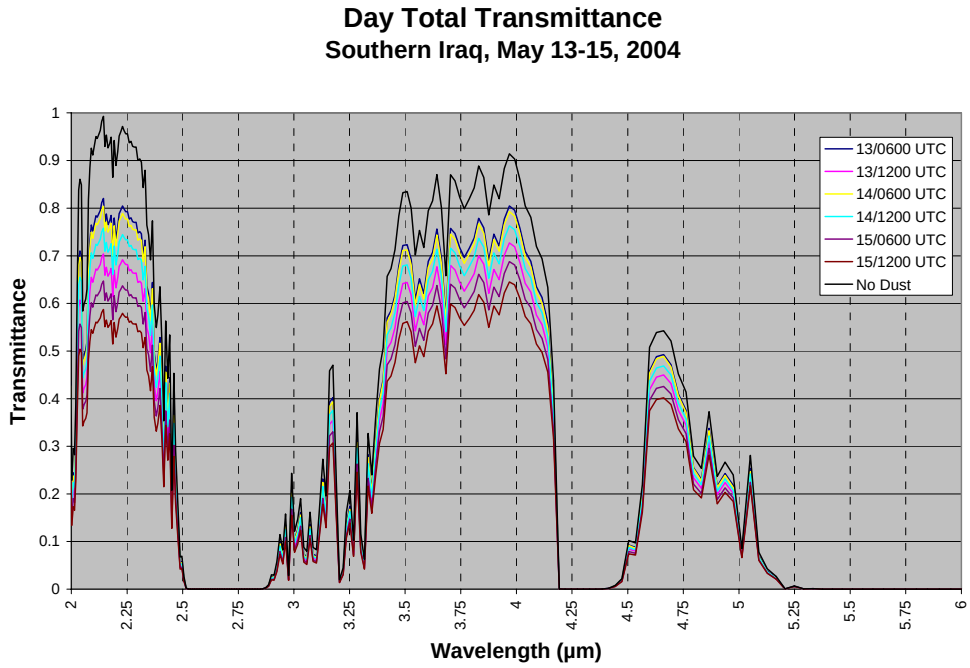

Figure 15. Transmittance - Iraq Case Study

The radiance values calculated for each day/time step and are shown in Fig. 16. A "No Dust Day" value is also plotted with all MODTRAN user defined dust extinction values set to zero, leaving only molecular absorption. The solar zenith angle plays a large part in the total reflected radiance and accounts for much of the difference between wavelengths from 2 to 2.6 µm (below the 2.7 µm water vapor absorption band). The daylight time steps for this region are 0600 UTC and 1200 UTC.

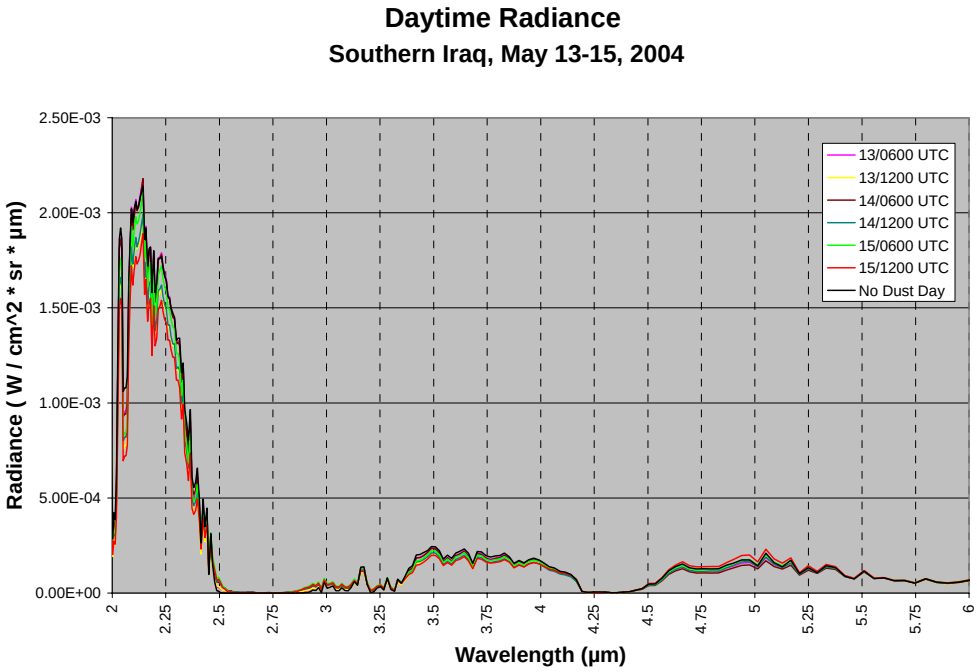

Figure 16. Iraq Total Daytime Radiance

Like the North Korea case, the variation of the daytime radiance values in the 3 to 5 µm band again is relatively small. The greatest difference for the 3 µm wavelength occurs between May 15th at 0600 UTC and the No Dust case with a difference of 3.50×10^{-5} W m^{-2} sr^{-1} μm^{-1}. While the values are small, the smallest value is 42% smaller than the greatest. At 4 µm, the smallest value is 17% smaller than the greatest, and at 5 µm the smallest value is 27% smaller than the greatest value.

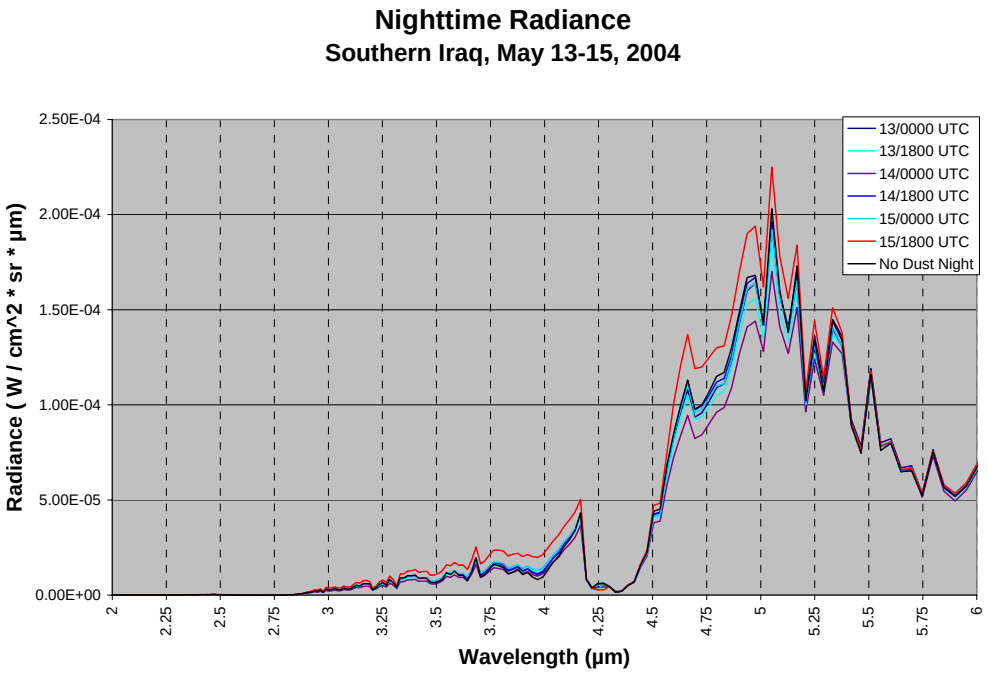

Figure 17. Iraq Total Nighttime Radiance

For the night time steps shown in Fig. 17, the solar component is completely absent and the only available radiance is due to the surface and path terms. Here the larger modeled radiance values on May 18th at 1800 UTC result from the warmest average column temperature and a 1.45 optical depth. The warm thermal characteristics for the column and heavy mass concentration allow the dust to absorb and emit more than the other days.

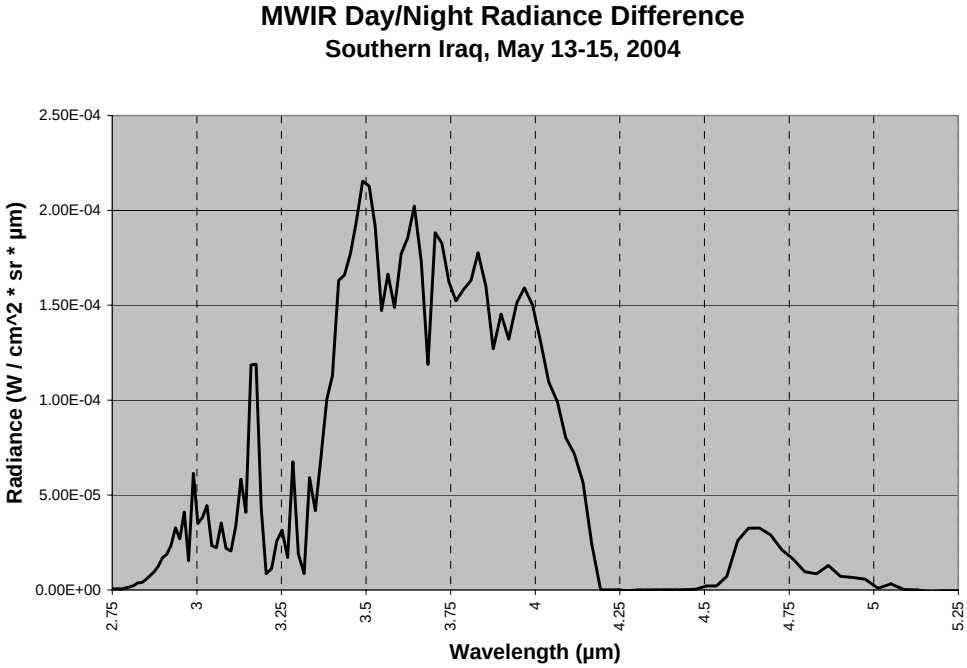

Figure 18. Average Day-Night Radiance Difference - Iraq Case

Figure 18 shows the difference between the day and night radiance values in the Iraq case study. The average solar contribution in the midwave bands was calculated as the difference between the daytime nighttime radiances. The greatest day/night radiance difference occurred at 3.49 µm with the average daytime radiance representing a 97% increase over the average nighttime radiance values. This further exemplifies the complexities of the midwave infrared region resulting from diurnal variability of radiance.

B. FIXED ATMOSPHERE CASES

1. Korean Peninsula

This case focused on the Korean Peninsula in central North Korea. The dust cases are based on the average atmospheric and dust mass concentration values modeled from March 20th, 2002 at 0000 UTC through March 23rd, 2002 at 1200 UTC.

a. Idealized Atmosphere

The need to isolate the effect of dust on the measured radiance values brought about the need to develop standard atmospheric profiles for each of the areas of interest. Once average profiles were developed, the extinction values could be modified to create idealized cases for light, moderate, and heavy mass concentrations as well as low, medium, and high dust altitude regions.

Each of the atmospheric parameters for all time steps within the case study was averaged to generate an "average" atmosphere, all of which could be treated as static parameters within MODTRAN. This allowed isolation of the dust vertical height and concentration as well as the time of day to derive radiance differences due solely to dust. Table 6 lists the static parameters used for the following calculations.

Table 6. Average Atmosphere - North Korea Idealized Case

Level	Layer dz (m)	Temp (K)	Pressure (mb)	Height (km)
1	33.44	278.38	944.75	0.017
2	70.49	278.02	936.60	0.069
3	109.00	277.00	924.09	0.158
4	147.91	275.91	907.32	0.287
5	227.31	275.67	882.11	0.475
6	301.70	273.79	849.51	0.739
7	372.24	271.73	810.66	1.076
8	440.96	269.05	766.50	1.483
9	508.23	266.19	718.07	1.957
10	576.01	263.80	666.43	2.499
11	640.22	259.90	612.60	3.107
12	706.24	256.43	557.55	3.781
13	768.71	252.39	502.39	4.518
14	831.30	248.60	448.09	5.318
15	887.61	244.63	395.78	6.178
16	923.41	237.15	346.41	7.083
17	944.74	230.21	301.02	8.017
18	939.64	223.35	260.65	8.959
19	988.48	217.70	223.13	9.923
20	1054.63	214.43	188.54	10.945
21	1152.12	214.11	156.79	12.048
22	1273.92	214.36	127.89	13.261
23	1412.82	213.63	101.92	14.605
24	1588.20	213.05	78.90	16.105
25	1833.99	213.60	58.71	17.816

b. Extinction Curves

The following extinction curves were created manually with the objective of placing the dust within specific vertical bins while achieving aerosol optical depths of light, moderate, and heavy corresponding to values of 0.5, 1.0, and 1.5, respectively. The height bins were determined by using the highest and lowest values observed in the Korean Peninsula case study in section A, and range from 1.5 to 6 km.

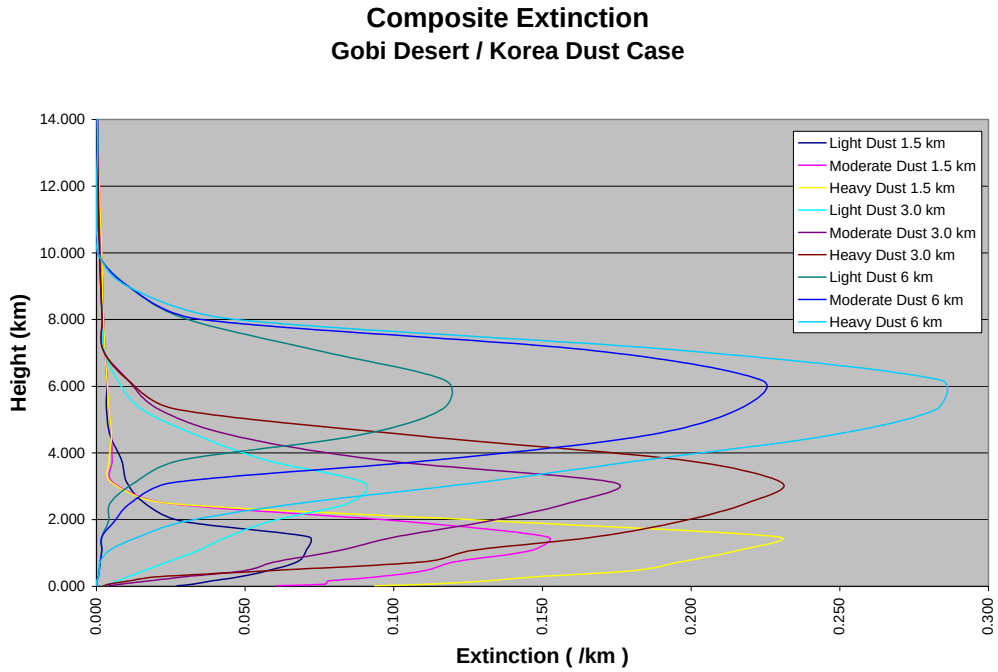

Figure 19. Idealized Dust Extinction and Height Curves - Korean Peninsula

Figure 19 depicts the manually generated extinction curves for the Korean Peninsula idealized case. A separate MODTRAN radiative transfer model run was accomplished for each curve for both a day and a night scenario. In addition, a case involving no dust was also run to measure the impact of dust on radiance and subsequent brightness temperature calculations.

c. Radiance

The following radiance values were calculated based on the average atmosphere and a 280 K surface temperature. Absorbing dust was assumed and multiple scattering with four streams was used for the MODTRAN calculations.

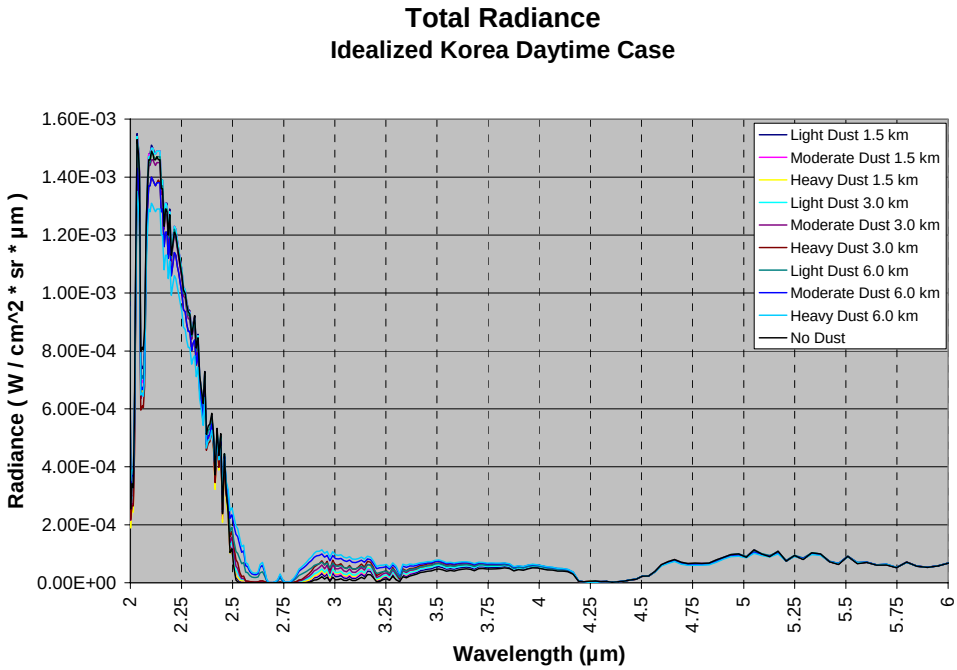

Figure 20. North Korea Variable Dust Daytime Total Radiance Output

The greatest total radiance produced for the midwave infrared in this case was the heavy dust at 6.0 km and was localized at the 3 µm end of the spectrum. With the solar irradiance still having a significant impact at wavelengths shorter than 4 µm, the highest and most dense dust receives more incident solar radiation thereby reflecting more solar radiation back to the sensor. The heavy dust continued to produce the greatest radiance through 4.185 µm where the carbon-dioxide absorption band reduced all values to near zero. As the wavelength exceeded 4.5 µm, the "No Dust" case produced the greatest values allowing the most terrestrial emittance through the atmosphere, though the difference between the greatest and least radiance was extremely small ($\leq$ 1 K). Of note, the water vapor absorption band centered at 2.7 µm shows variability due to more water

vapor lower than the 6 km dust. This allowed the heavy 6 km dust to continue to reflect some incident solar irradiance. Heavy dust loading at higher altitudes resulted in greater radiance values at wavelengths shorter than 2.97 μm where heavy dust loading at 3.0 km resulted in greater radiance values than light dust loading at 6.0 km. This is a result of the light 0.5 AOD dust at 6.0 km losing enough solar reflectance to the point where the heavy 1.5 AOD dust at 3.0 km made up the difference with greater thermal emission but reduced reflective properties.

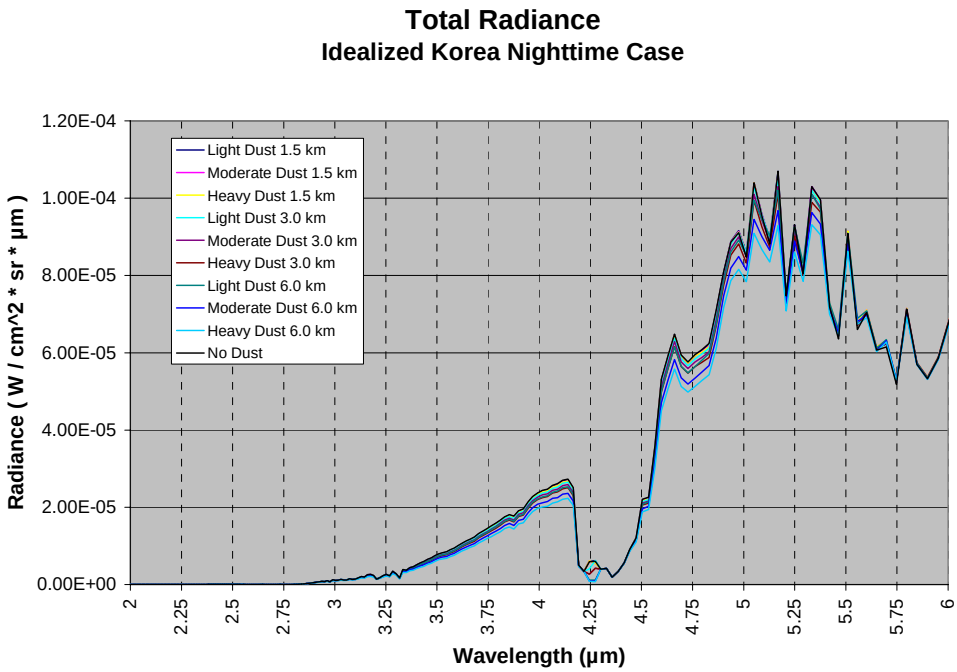

Figure 21. North Korea Variable Dust Nighttime Total Radiance Output

The night radiance graph shown in Fig. 21, allows closer inspection of the thermal end of the spectrum. This gives a better look at the impact of the thermal emissivity and associated dust impacts at longer wavelengths. Since the solar radiances are no longer dominating, there is no perceptible measurable radiance at wavelengths shorter than 2.5 μm. The radiance differences here are solely dependent on the absorptive/emissive properties of the dust and the thermal character of the surrounding atmosphere.

In this case, the greatest value within the 3-5 μm range was the "No Dust" case with heavy dust loading at 6 km representing the smallest value. Since this was a springtime case, the elevated dust will emit at a cooler temperature due to the 250 K temperature at 6.0 km. The greatest radiance is due to emission by the greater surface temperature transmitting through an atmosphere with no dust. These are small differences relative to the daytime condition but become more significant when calculating brightness temperature.

d. Brightness Temperature

Brightness temperature was calculated based on the inverted Planck Function. All values in the figures below correspond directly to the radiance values in Figures 20 and 21.

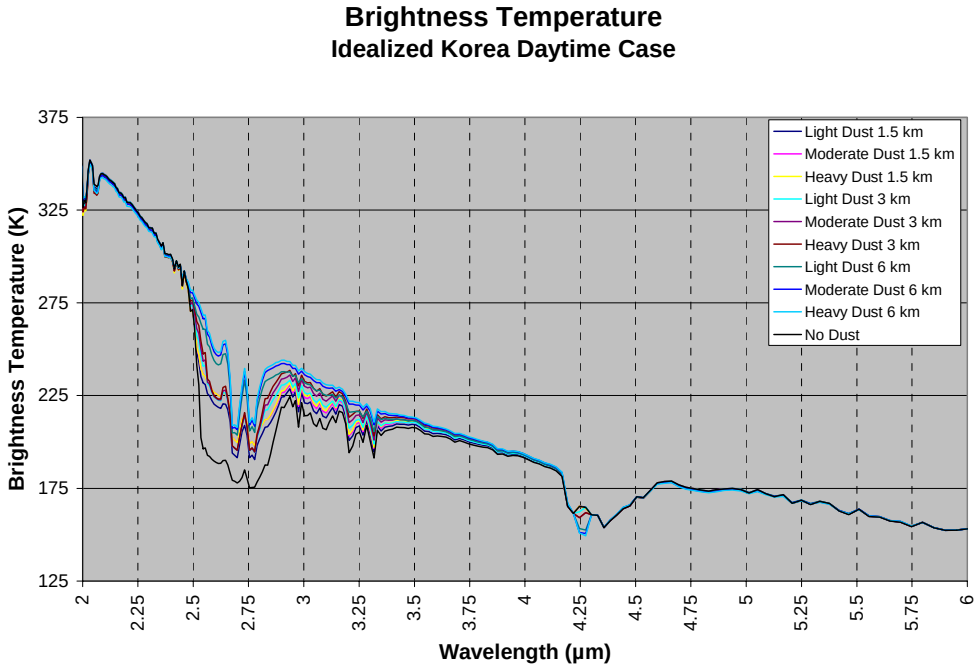

Figure 22. North Korea Variable Dust Daytime Brightness Temperature

Although the radiance values showed small differences between the "No Dust" and differing aerosol optical depths and heights, the brightness temperatures show much greater differences due to the nonlinear nature of the Planck Function. The greatest difference within the midwave band for this case occurred at 3.0 μm where heavy dust loading at 6.0 km was 18.6 K warmer than the No Dust case - an 8% increase for heavy dust over the "No Dust" case. This is indicative of solar irradiance reflection off of the dust layer and increased top of the atmosphere radiance. The effect was similar with brightness temperature differences decreasing up to 4 μm where carbon-dioxide absorption reduced all values. Beyond 4.7 μm there were only fractional differences in brightness temperature. Table 7 shows the greatest differences for each 1/4 μm of the midwave infrared.

Table 7. Brightness Temperature Differences For Midwave Infrared Wavelengths During the Idealized Korean Day Scenario

Wavelength (μm)	**Coldest Temp**	**Tb (Kelvin)**	**Warmest Temp**	**Tb (Kelvin)**	**Difference (Kelvin)**
6.006	Heavy-High	153.175	Moderate/Heavy-Low	153.294	0.119
5.747	No Dust	154.315	Heavy-High	154.643	0.328
5.510	Heavy-High	163.508	Light-High	163.805	0.297
5.249	Heavy-High	168.194	Light-High	168.680	0.486
5.013	Heavy-High	172.139	Light-High	172.699	0.560
4.762	Heavy-High	173.789	Light-Low	174.900	1.111
4.505	Heavy-Mid	170.177	Light-High	170.530	0.353
4.246	Heavy-High	150.826	Moderate/Heavy-Low	165.523	14.697
3.992	No Dust	191.709	Heavy-High	193.886	2.177
3.745	No Dust	198.964	Heavy-High	202.720	3.756
3.490	No Dust	207.838	Heavy-High	213.465	5.627
3.252	No Dust	205.284	Heavy-High	221.147	15.863
3.003	No Dust	221.151	Heavy-High	239.722	18.571
2.755	No Dust	175.291	Heavy-High	210.560	35.269
2.554	No Dust	196.771	Heavy-High	268.484	71.713
2.497	No Dust	271.352	Heavy-High	281.823	10.471
2.252	Heavy-High	321.272	Light-Low	323.629	2.357
2.002	Heavy-Low	322.189	Heavy-High	331.350	9.161

Toward shorter wavelengths of the midwave IR, brightness temperature fluctuations become larger due to increased reflected solar radiation. These differences

decrease in the window wavelengths. Water vapor and carbon-dioxide absorption have a significant impact at and just below 2 µm. The significant brightness temperature differences for the Korea Day case occur from 2.5 to 4 µm. At 4.25 µm there is a carbon-dioxide absorption band which impacts brightness temperature measurement by absorbing low level radiation. When the dust becomes sufficiently elevated, the upper portions of the dust layer are high enough to radiate photons to the top of the atmosphere. The heavy dust loading at high altitudes and colder temperatures produces cooler brightness temperatures. The lower dust layers become obscured by carbon-dioxide absorption.

Average brightness temperature ranged from 172.7 to 233.2 K with the largest standard deviation of 14.1 at 2.55 µm outside the midwave spectrum and 7.60 K at 3.2 µm within the midwave spectrum. The variance is reduced to less than 1 K at 3.70 µm and remains less than 1 K through the rest of the midwave, with the exception of the 4.24 to 4.27 µm band where there is a 6 to 6.5 K variance due to carbon dioxide absorption.

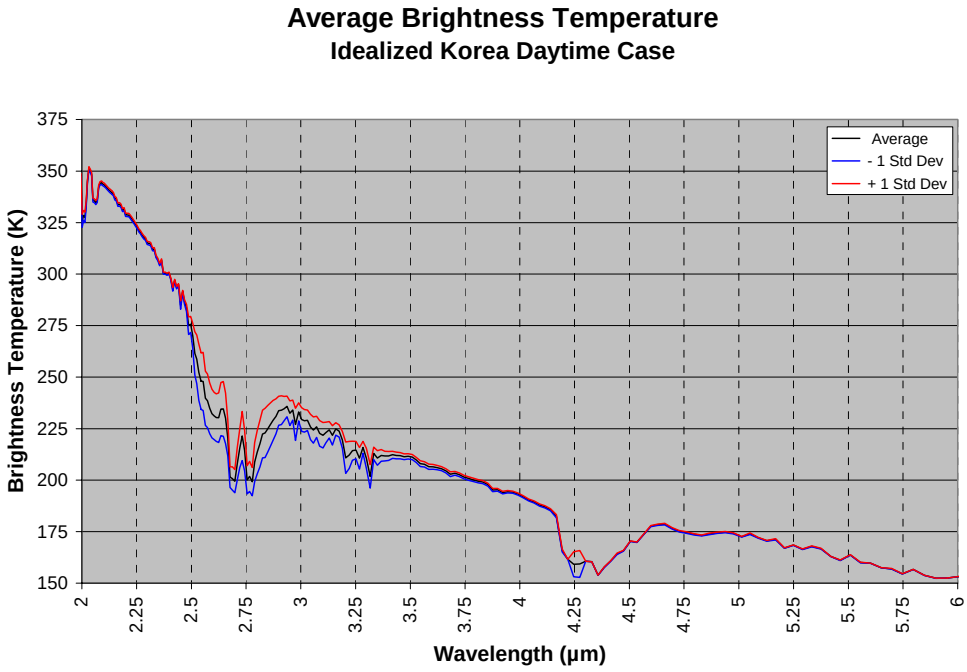

Figure 23. North Korea Variable Dust Daytime Average Brightness Temperature

For an atmosphere with no dust, the wavelength where the MODTRAN defined surface temperature of 280 K was most closely observed was roughly 2.478 μm. The average temperature of all cases at this wavelength was 281.80 K and the variance was 1.7 K. Significant variances within the 2.7 μm water vapor absorption band were observed with values greater than 5 K in the range of 2.5 to 3.1 μm. In this range, the greatest brightness temperature was consistently the heavy dust loading at 6.0 km and the smallest were the "No Dust" case and light dust loading at 1.5 km. This is a result of less intervening water vapor between the elevated dust and the top of the atmosphere, thus allowing solar reflected radiation through to the dust and back to the sensor.

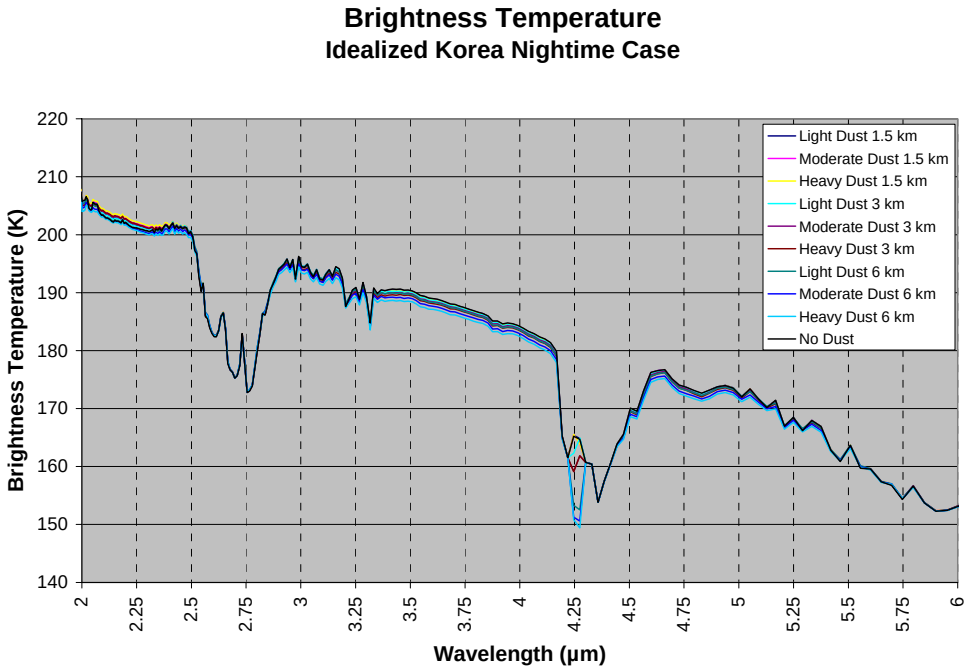

Figure 24. North Korea Variable Dust Nighttime Brightness Temperature

Nighttime brightness temperatures exhibited far less variability but more consistent differences across the midwave spectrum. The spectral brightness temperature graph in Fig. 24 shows the variability and Table 8 shows fairly consistent temperature variability from 0.9 K at 5.013 μm to 1.9 K at 3.49 μm. Again, the carbon-dioxide

absorption band brings a large 14 to 15 K difference from 4.24 to 4.27 μm. The "No Dust" case showed the warmest temperature throughout (excluding the carbon dioxide absorption band) and the heavy dust loading at 6.0 km was consistently the coldest.

At virtually all midwave wavelengths (except the carbon dioxide absorption band), brightness temperature ranged from warmest to coldest in order of dust height and loading as follows:

No Dust	
Light Dust	1.5 km
Moderate Dust	1.5 km
Heavy Dust	1.5 km
Light Dust	3.0 km
Moderate Dust	3.0 km
Light Dust	6.0 km
Heavy Dust	3.0 km
Moderate Dust	6.0 km
Heavy Dust	6.0 km

Table 8. Brightness Temperature Differences for Midwave Infrared Wavelengths During the Idealized Korean Night Scenario

Wavelength (μm)	**Coldest Temp**	**Tb (Kelvin)**	**Warmest Temp**	**Tb (Kelvin)**	**Difference (Kelvin)**
6.006	Heavy-High	153.095	Light/Mod/Heavy - Low/Mid	153.135	0.040
5.747	No Dust	154.315	Mod/Heavy Low, Mod-High	154.480	0.165
5.510	Heavy-High	163.125	Mod/Heavy-Low	163.732	0.607
5.249	Heavy-High	167.645	Light-Low, No Dust	168.480	0.835
5.013	Heavy-High	171.193	Light-Low	172.139	0.946
4.762	Heavy-High	172.142	Light-Low	173.642	1.500
4.505	Heavy-High	168.602	No Dust	170.077	1.475
4.274*	Heavy-High	149.409	Light-Low	164.847	15.438
4.246	Heavy-High	150.826	Mod/Heavy-Low	165.523	14.697
3.992	Heavy-High	182.578	No Dust	184.310	1.732
3.745	Heavy-High	185.623	No Dust	187.446	1.823
3.490	Heavy-High	188.540	No Dust	190.450	1.910
3.252	Heavy-High	189.274	No Dust	190.903	1.629
3.003	Heavy-High	194.406	No Dust	196.255	1.849
2.755	No Dust	172.766	Mod/Heavy-Low	172.847	0.081
2.497	Heavy-High	199.556	Light-Low	200.694	1.138
2.252	Heavy-High	200.704	Heavy-Low	202.203	1.499
2.002	Heavy-High	204.007	No Dust	205.781	1.774

Table 8 provides a tabular snapshot at roughly 1/4 μm increments brightness temperature differences. There were very consistent values within the midwave IR region. Heavy dust loading at high altitudes was consistently the coldest temperature due to the cool temperatures of the emitting layer.

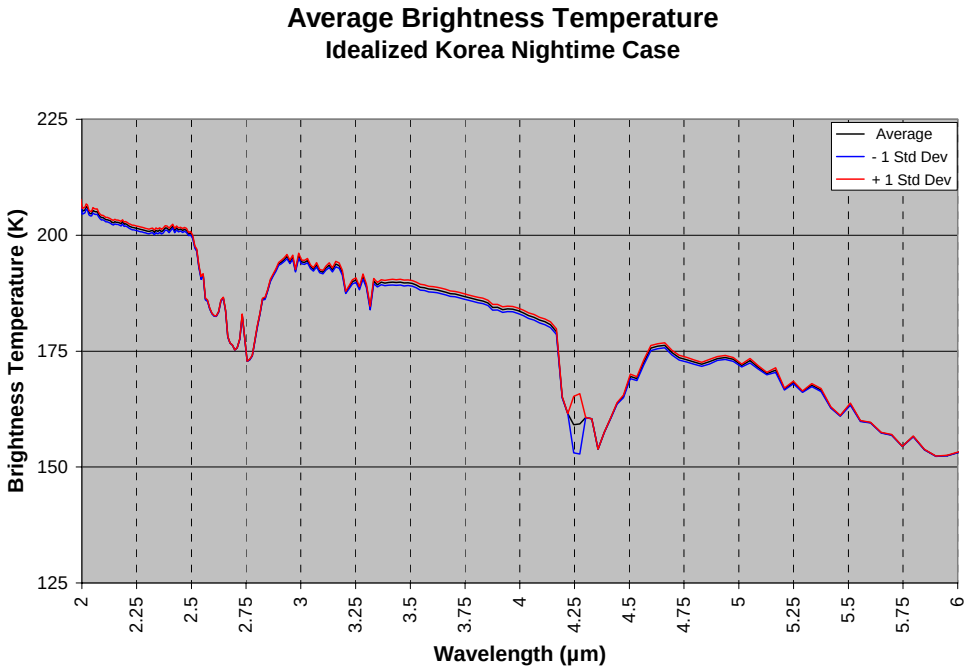

Figure 25. North Korea Variable Dust Nighttime Average Brightness Temperature

The night average radiance values exhibited much less spectral variability and much less variance between cases. Since there is no reflected solar radiation, and the wavelength is too short to exhibit significant emissive properties, the large variance values seen in the water vapor absorption band during the daytime cases are eliminated. All water vapor absorption band cases had less than 0.5 K variance between 2.5 and 3 μm.

2. Iraq Desert

This case focused on the desert of Iraq toward the Tigris-Euphrates River Valley. The dust cases are based on the average atmospheric and dust mass concentration values modeled from May 13, 2004 at 0000 UTC through May 15, 2004 at 1800 UTC.

a. Idealized Atmosphere

As with the Korean Peninsula case, a pseudo-standard atmospheric profile was used for this area of interest, average profiles were developed, and the extinction values were modified to create idealized cases for light, moderate, and heavy mass concentrations as well as low, medium, and high dust altitude regions.

Table 9. Average Atmosphere - Iraq Desert Idealized Case

Level	Layer dz (m)	Temp (K)	Pressure (mb)	Height (km)
1	36.14	300.88	976.17	0.018
2	76.98	303.58	967.75	0.075
3	119.34	303.27	954.83	0.173
4	162.16	302.47	937.50	0.314
5	248.12	300.90	911.45	0.519
6	328.98	298.54	877.76	0.807
7	404.87	295.54	837.62	1.174
8	478.12	291.71	791.99	1.616
9	548.86	287.46	741.95	2.129
10	618.27	283.14	688.59	2.713
11	684.82	277.99	632.97	3.364
12	751.40	272.81	576.08	4.082
13	812.57	266.77	519.09	4.864
14	872.57	260.92	462.98	5.707
15	923.38	254.47	408.93	6.605
16	962.55	247.18	357.91	7.548
17	983.57	239.64	311.01	8.521
18	977.69	232.36	269.30	9.502
19	1022.96	225.27	230.52	10.502
20	1090.08	221.61	194.78	11.558
21	1182.64	219.74	161.98	12.695
22	1283.08	215.85	132.11	13.928
23	1381.83	208.88	105.28	15.260
24	1519.48	203.76	81.49	16.711
25	1751.21	203.86	60.63	18.346

Table 9 identifies the static atmospheric profile for the Iraq Desert case using the average NAAPS output for each variable. The column temperature was significantly warmer, which one would expect given the geographic region and the later spring date.

b. Extinction Curves

The following extinction curves were created manually with the objective of placing the dust within specific vertical bins while achieving aerosol optical depths of light, moderate, and heavy corresponding to values of 0.5, 1.0, and 1.5 respectively. The height bins were determined by using the highest and lowest values observed in the Iraq Desert case study in section A and altitudes range from 1.5 to 5 km.

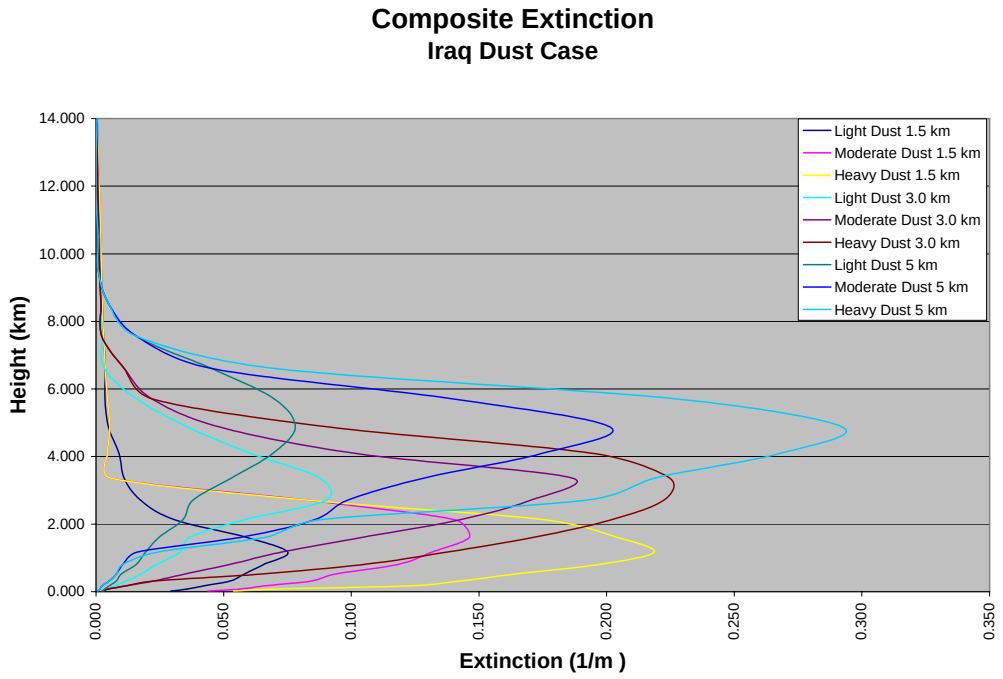

Figure 26. Idealized Dust Extinction and Height Curves - Iraq Desert

Figure 26 depicts the manually generated extinction curves for the Iraq Desert idealized case. Like the Korean Peninsula case, a separate MODTRAN radiative

transfer model run was accomplished for each curve for both a day and a night scenario. In addition, a case involving no dust was also run to measure the impact of dust on radiance and subsequent brightness temperature calculations.

c. Radiance

The following radiance values were calculated based on the average atmosphere and a 300 K surface temperature. Absorbing dust was assumed and multiple scattering with four streams was used.

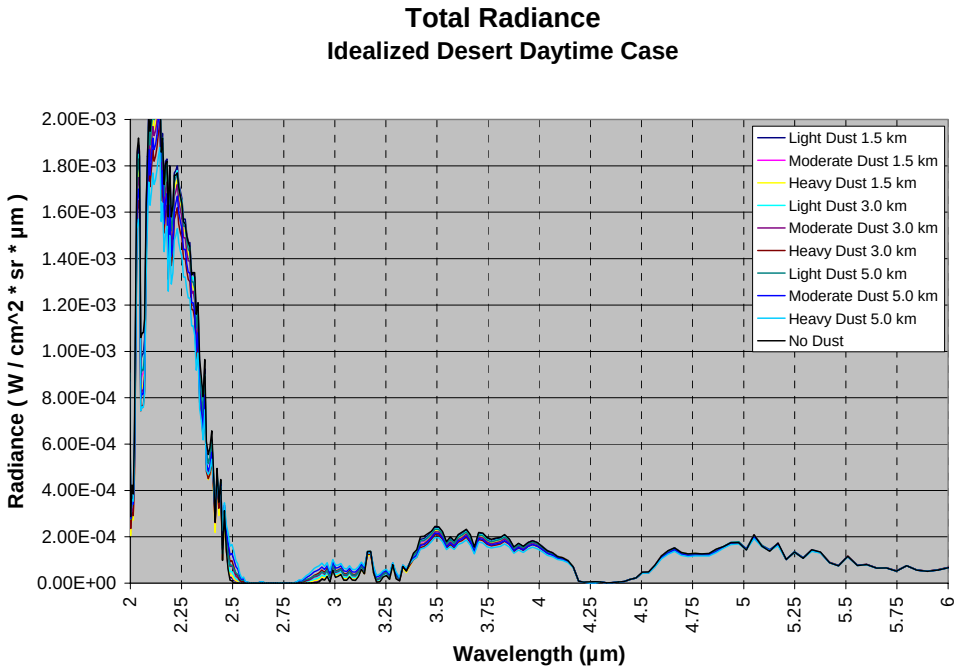

Figure 27. Southern Iraq Variable Dust Daytime Total Radiance Output

In Fig. 27 the radiance values again showed small differences between the "No Dust" and differing aerosol optical depth and heights. These radiance values translate to greater brightness temperature values through conversion in the Planck Function. For wavelengths shorter than 3.3 µm, the warmest temperature was represented by the heavy dust loading at 5.0 km due to the increase in solar reflectance by the heavy-elevated dust. This occurs at a much shorter wavelength than the Korean Peninsula case due to the warmer surface/low level temperatures and less albedo

difference between the desert surface and the elevated dust. The "No Dust" case was consistently warmer in the spectral bands longer than 3.3 µm. At wavelengths longer than the 4.2 µm carbon dioxide band, radiance differences became very small due to less impact of dust sized particles on longer wavelength radiation.

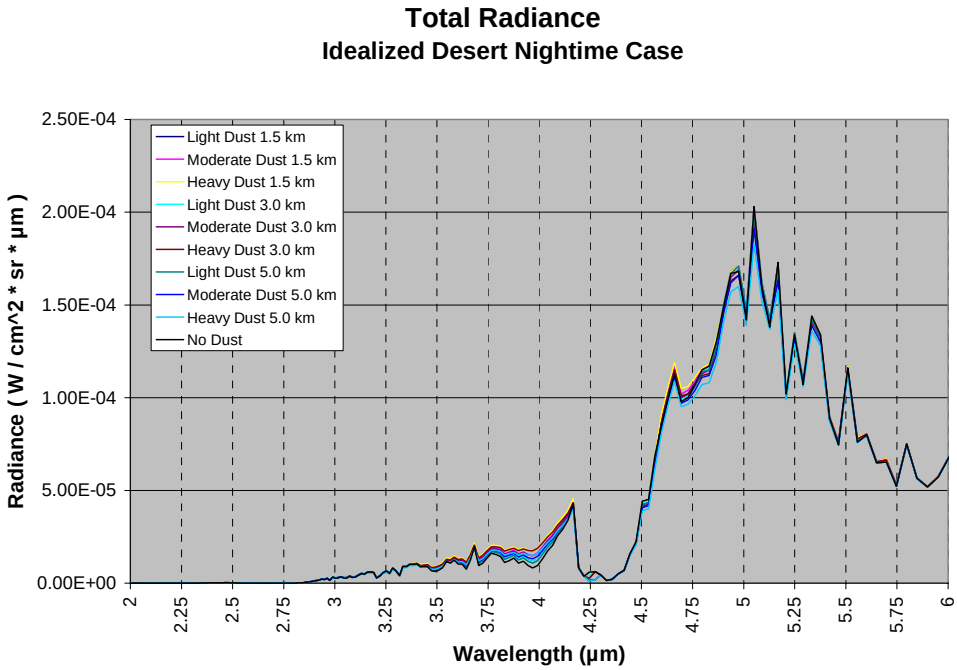

Figure 28. Southern Iraq Variable Dust Nighttime Total Radiance Output

The night radiance graph shown in Fig. 28, allows us to scale closer to see the thermal end of the spectrum giving a better look at the impact of the thermal emissivity and associated dust impacts. Since the solar radiances are no longer dominating, there is no perceptible measurable radiance at wavelengths shorter than 2.5 µm. The radiance differences here are solely dependent on the absorptive properties of the dust and the thermal character of the atmosphere in which they occupy.

In this case, the greatest value within the 3 to 5 µm range was the heavy dust loading at 1.5 km. This was puzzling until the temperature profile used was closely examined. In this case, the low level temperatures are warmer than the surface temperature and therefore the dust at the lower levels will emit at warmer temperatures

than the surface and the elevated dust. For that reason, all dust layers produced greater radiance values than the "No Dust" case between 3 and 4.25 μm. At wavelengths longer than 4.25 μm, the "No Dust" case returned the greatest radiance values.

d. Brightness Temperature

Brightness temperature was calculated based on the inverted Planck Function. All values correspond directly to the radiance values in Figures 27 and 28.

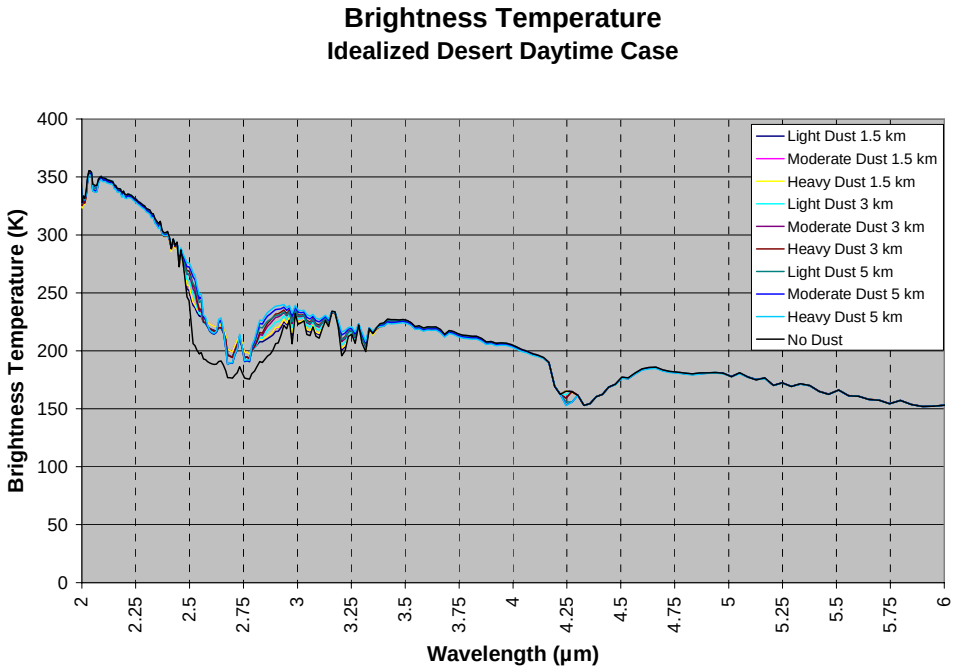

Figure 29. Southern Iraq Variable Dust Daytime Brightness Temperature

Although the radiance values showed small differences between the "No Dust" and differing aerosol optical depth and heights, the brightness temperatures show much larger differences due to the Planck Function. The greatest difference within the midwave band for this case occurred at 3.0 μm where heavy dust loading at 6.0 km was 12.4 K warmer than the No Dust case. That is a 5.3% increase for heavy dust over the "No Dust" case. This is an important area in the midwave due to its proximity to the

water vapor absorption band in the 2 to 3 μm region. Atmospheric water vapor still has some effects at 3 μm and lower dust will have more water vapor above it to absorb solar radiation thus reducing the solar irradiance incident on the dust and thereby reducing the reflectance to the sensor. Additionally, the elevated dust at a wavelength of 3 μm continued to have the highest brightness temperature up to 3.5 μm where the solar and terrestrial dominance switched causing the warmest brightness temperature beyond 3.5 μm to come from the "No Dust" case. More terrestrial radiation and greater near-surface temperatures made the low dust or the "No Dust" cases produce warmer brightness temperatures through the 5 μm band. At 4.25 μm, the carbon-dioxide absorption band reduced all temperatures, but the 5.0 km dust layer produced coldest values due to its elevated level above enough of the carbon dioxide to radiate at colder temperatures. Beyond 4.7 μm there were only fractional differences in brightness temperature. Table 10 shows the greatest differences for each 1/4 μm increment of the midwave infrared.

Table 10. Brightness Temperature Differences For Midwave Infrared Wavelengths During the Idealized Iraq Day Scenario

Wavelength (μm)	**Coldest Temp**	**Tb (Kelvin)**	**Warmest Temp**	**Tb (Kelvin)**	**Difference (Kelvin)**
6.006	Heavy-High	153.175	Mod/Heavy-Low	153.254	0.079
5.747	Heavy-High	153.370	Mod/Heavy-Low	154.589	0.219
5.51	Heavy-High	165.979	Mod/Heavy-Low	166.281	0.302
5.249	Heavy-High	172.133	Light-High	172.457	0.323
5.013	Heavy-High	177.610	Light-High	178.029	0.419
4.762	Heavy-High	180.604	Light/Heavy-Low	181.624	1.020
4.505	Heavy-High	176.253	No Dust	177.208	0.956
4.246	Heavy-High	152.527	Light/Mod/Heavy-Low & No Dust	165.523	12.996
3.992	Heavy-High	203.357	Light-Low	205.296	1.939
3.745	Heavy-High	212.160	No Dust	214.796	2.636
3.49	Heavy-High	224.316	No Dust	227.031	2.715
3.252	No Dust	214.297	Heavy-High	220.591	6.294
3.003	No Dust	222.874	Heavy-High	235.231	12.357
2.755	No Dust	176.558	Mod/Heavy-Low	198.075	21.518
2.516	No Dust	206.219	Heavy-High	267.456	61.237
2.497	No Dust	243.117	Heavy-High	275.843	32.726
2.252	Light-Low	327.971	Heavy-High	330.815	2.844
2.002	Heavy-Low	323.377	Heavy-High	329.154	5.776

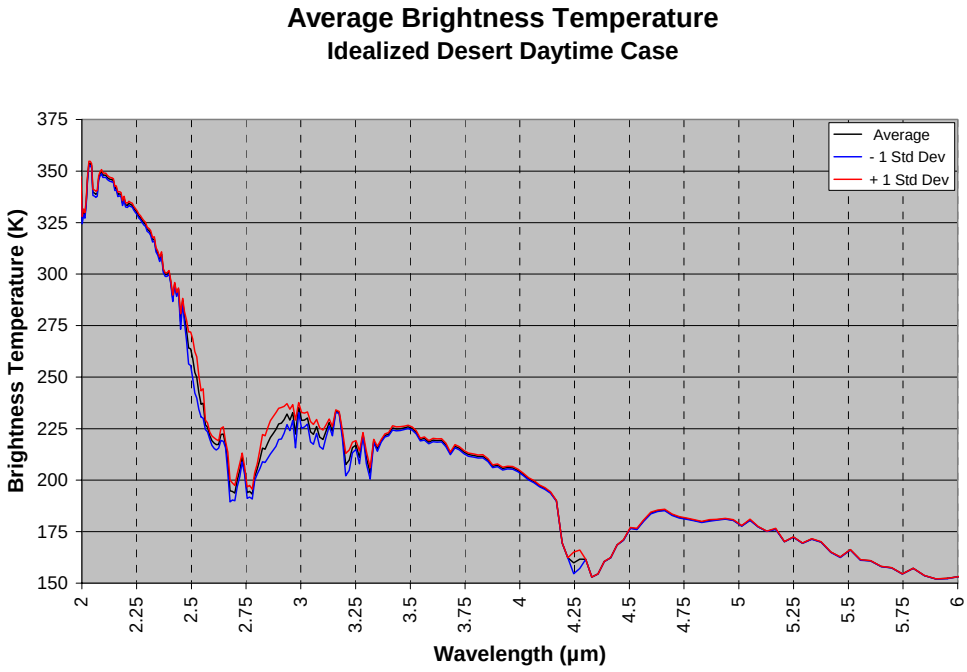

Figure 30. Southern Iraq Variable Dust Daytime Average Brightness Temperature

The average brightness temperature and one standard deviation for the daytime Iraq scenario are plotted in Fig. 30. The greatest variance in the midwave occurred at the shortest wavelengths with a standard deviation of 4.9 K at 3.04 µm. Other notable variances were observed at 3.2 µm with a variance of 5.4 K and at 4.2 µm in the carbon-dioxide absorption band with a variance of 5.2 K.

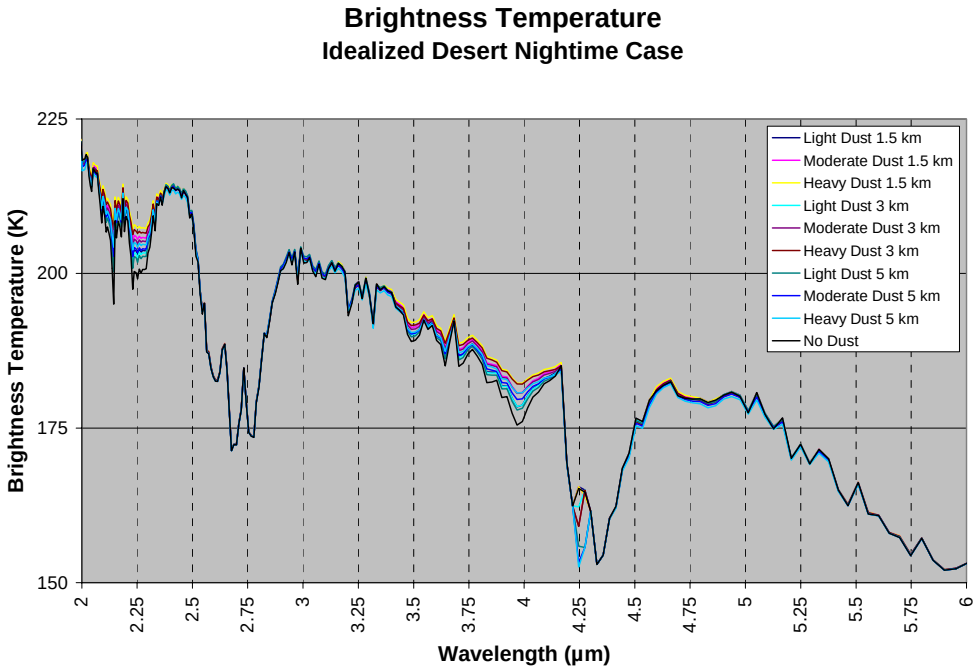

Figure 31. Southern Iraq Variable Dust Nighttime Brightness Temperature

Nighttime brightness temperatures exhibited less variability and more consistent differences across the midwave spectrum. The low-level thermal inversion made the 1.5km dust warmer than all other cases. The greatest variability within the midwave infrared spectrum for this case (excluding the carbon-dioxide band) occurred at 3.96 µm where the heavy dust loading at 1.5 km was 6.7 K warmer than the "No Dust" condition, as a result of the low-level thermal inversion. The spectral graph in Fig. 31 shows the variability between the dust cases and the "No Dust" case and Table 11 shows fairly consistent temperature variability above 4.5 µm with differences below 1.3 K. At wavelengths shorter than 4 µm the differences ranged from 1.2 K at 3 µm to 6.7 at 3.96 µm.

This case underscored the importance of the low-level temperature profile. The data indicate that heavy dust loading in the low levels can make interpreting the surface temperature quite difficult in the presence of a temperature inversion.

Table 11. Brightness Temperature Differences For Midwave Infrared Wavelengths During the Idealized Iraq Night Scenario

Wavelength (μm)	Coldest Temp	Tb (Kelvin)	Warmest Temp	Tb Kelvin)	Difference (Kelvin)
6.006	Heavy-High	153.175	Mod/Heavy-Low	153.254	0.079
5.747	Heavy-High	154.370	Mod/Heavy-Low	154.589	0.219
5.51	Heavy-High	165.887	Light-Low	166.251	0.364
5.249	Heavy-High	171.923	Light-Low	172.428	0.504
5.013	Heavy-High	177.239	Light-High	177.851	0.612
4.762	Heavy-High	179.081	Heavy-Low	180.06	0.979
4.505	Heavy-High	175.365	No Dust	176.584	1.219
4.246	Heavy-High	152.527	Light-Low	165.523	12.996
3.992	No Dust	176.049	Heavy-Low	182.249	6.200
3.745	No Dust	186.937	Heavy-Low	189.628	2.690
3.49	No Dust	188.999	Heavy-Low	192.094	3.095
3.252	Heavy-Mid	198.093	Light-Low	198.711	0.617
3.003	No Dust	201.680	Light-High	202.801	1.122
2.755	No Dust	174.305	Mod/Heavy-Low	174.415	0.111
2.497	Light-High	209.313	Heavy-High	210.212	0.899
2.252	No Dust	199.169	Heavy-Low	207.299	8.130
2.002	Heavy-High	216.635	Light-Low	218.309	1.674

The values in Table 11 represent each 1/4 μm increment maximum brightness temperature difference from all cases in the Iraq nighttime scenario. Due to the low-level thermal inversion and the warmer low-level temperatures, the warmest temperatures were for the dust rather than the "No Dust" case. The results indicate that a nocturnal inversion will make the emission from dust layers greater at midwave infrared wavelengths. With the exception of the carbon dioxide absorption band, where the low-level dust is not able to emit to the top of the atmosphere, the 1.5 km dust was consistently warmer.

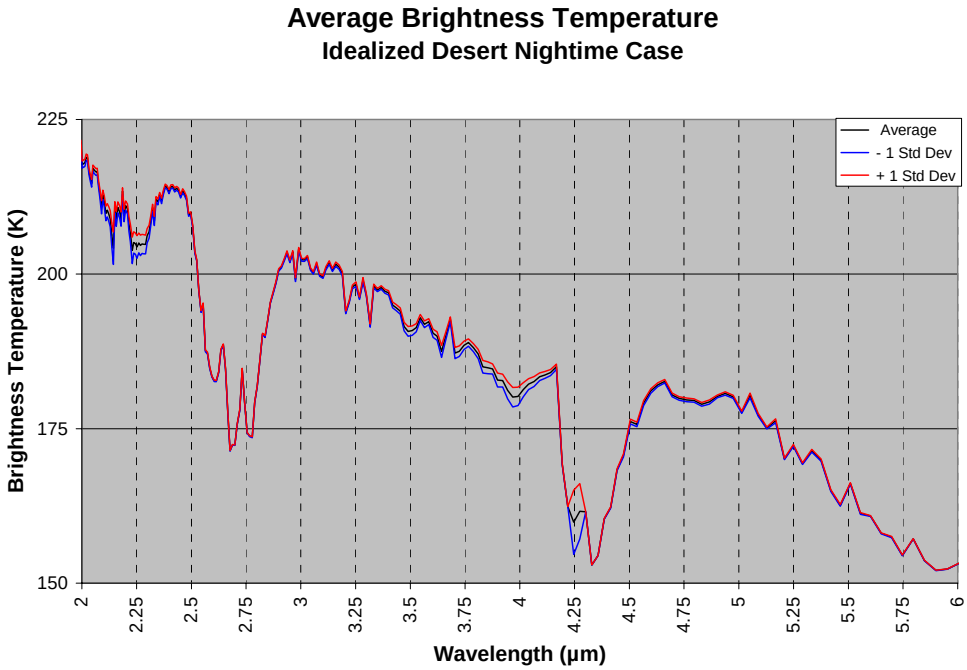

Figure 32. Southern Iraq Variable Dust Nighttime Average Brightness Temperature

The average brightness temperature, and plus/minus one standard deviation for the nighttime Iraq scenario are plotted in Fig. 32. The greatest variance in the midwave occurred from 3.8 to 4.0 µm with a standard deviation of 1 to 1.5 K and in the carbon dioxide absorption band with a variance of 3.0 to 5.2 K. The variance beyond 4.3 µm was below 0.4 K.

VI. CONCLUSIONS AND RECOMMENDATIONS

A. CONCLUSIONS

The objective of this study was to determine the vertical variation of dust during dust events over operationally significant regions and the subsequent impact that variation has on the top of the atmosphere radiance and brightness temperature in the midwave infrared spectrum.

The NAAPS global aerosol model dust mass concentration was used to determine how dust varies vertically during a given dust event through vertical extinction. The NAAPS dust data along with the corresponding atmospheric data of two dust events were used in conjunction with the MODTRAN radiative transfer software to generate the impact of varying the height and aerosol optical depth on top of the atmosphere radiance and brightness temperature producing the following results.

1. Vertical Variation of Dust

The extinction curves indicate that the heavy mass concentration dust modeled from the Gobi Desert over the Korean Peninsula varied from 1 to 6 km using the 25 layer NAAPS model. Above 6 km the mass concentration and extinction values dropped exponentially with height with extinction values of less than 0.05 m^{-1} above 6 km. It is important to note the NAAPS model layers correspond to the NOGAPS sigma coordinate system, thus vertical resolution decreases with height.

The extinction curves in the Iraq desert case indicate that the heavy mass concentration dust modeled from the Tigris-Euphrates Alluvial Plain over southern Iraq varied from 1 to 5 km using the 25 layer NAAPS model. Again, above 5 km the mass concentration and extinction values dropped exponentially with height with extinction values of less than 0.05 m^{-1} above 5.25 km.

Factors most impacting the vertical variability of dust include the proximity of the measured dust to the source region, atmospheric dynamics including stability and vertical motion, and the composition of the dust including mass, number and size distribution.

Discussions with the NAAPS modeling group from the Naval Research Laboratory, Marine Meteorology Division, Monterey, CA, indicate there could be significant differences between using the OPAC based NAAPS model and other dust models due to differing size and number distribution characteristics as well as differing optical properties and meteorological forcing parameters. Results of a study undertaken by John McMillen in 2007 showed the differences between various dust optical property models to be significant, particularly between the default MODTRAN models and external models.

2. Impact of Vertically Varying Dust in Midwave Infrared Radiance and Brightness Temperature

Varying dust height while keeping temperature, pressure, and thickness static changed the modeled radiance and subsequent brightness temperature at the top of the atmosphere. The aerosol optical depth and vertical height of the dust made dust more or less reflective in the solar irradiance influenced band between 3 and 4.25 μm which varied the brightness temperature greatly during daytime hours. Beyond the carbon-dioxide band at 4.25 μm, solar impacts were far less and the temperature of the dust layer and the surface temperature were dominant.

The greatest brightness temperature variability due to dust height and loading ranged from 2.1 to 18.6 K in Korea daytime case, 0.9 to 1.9 K in Korea nighttime case, 0.5 to 12.4 K in Iraq daytime case, and 0.6 to 6.2 K in Iraq nighttime case. Radiance and brightness temperature differences became relatively small ($\leq$ 1.5 K) beyond the 4.2 μm carbon-dioxide absorption band.

Measuring carbon dioxide absorption at 4.2 μm is not recommended during dust events as results will vary greatly with the height and mass concentration of the dust. In every case, the elevated dust produced a colder temperature than all other dust and non-dust events in the 4.25 μm band. The dust layers at 1.5 and 3.0 km were low enough to be within or below the highest/most elevated carbon-dioxide weighting function.

Significant differences from 13.0 to 15.4 K occurred within the carbon-dioxide absorbing band at 4.25 μm during both day and nigh scenarios. Differences from 61.2 to 71.7 K occurred within the water vapor absorbing band at 2.55 μm during the daytime scenario. These differences were the result of varying the height of dust above the weighting functions of the respective gases creating colder emission in the case of the elevated dust in the carbon-dioxide absorbing band and greater reflectance in the water vapor absorption band.

B. RECOMMENDATIONS

As a result of this study, the following recommendations are suggested:

- Repeat the study for differing optical properties of dust and differing low-level temperature profiles. Use of the NPS aerosol models, MODTRAN internal models, and the US Army dust optical models will help determine the inter-model variability in radiance and brightness temperature. Vary the atmospheric conditions to represent realistic seasonal and regime-specific vertical profiles of pressure, temperature, and thickness for the given areas of interest. Combining the best model with the best atmospheric representation will result in a better estimation of the impact of dust.
- Undertake a measured and modeled climatological study of the vertical variation of dust in the known source regions and downstream dust impacted regions incorporating LIDAR technology with various dust models. Exploit recent on-orbit LIDAR data availability from satellites such as CALIPSO and CloudSat. Compare these data with modeled NAAPS data to assess the accuracy of dust modeling. Using information on backscatter polarization will provide information about particle shape which will further improve the ability to model the dust.

- Use higher spatial and temporal resolution meteorological and dust models to study short lived, smaller events from concentrated point sources and better resolve the vertical height of dust in all regions. Inner nests of COAMPS and WRF/MM5 will provide resolution to capture events lasting less than 6 hours. Use of these high resolution models will provide much better vertical resolution to further quantify the vertical variation of dust as well as better horizontal resolution to better resolve the small dust events resulting from point sources.
- Verify the MODTRAN output in the midwave infrared spectrum using commercial and DOD satellite measurements. This can be accomplished by comparing brightness temperature output from MODTRAN to satellite measurements from MODIS, SeaWiFS, and AVHRR. Further research will allow gaseous constituents to be more accurately represented in MODTRAN resulting in a better representation of the background atmosphere.
- Create an automated process by which NAAPS or similar 3-D modeled dust data can be ingested into a radiative transfer algorithm such as MODTRAN to produce user-defined spectrally and geographically specific radiance/brightness temperature variability data in graphical form.

LIST OF REFERENCES

Air Force Research Laboratory Space Vehicles Directorate, cited February 2007: MODTRAN 4 Software. [Available online at http://www.vs.afrl.af.mil/ProductLines/IR-Clutter/modtran4.aspx].

Alley, R. E., M. Jentoft-Nilsen, 2001, Algorithm Theoretical Basis Document for Brightness Temperature Version 3.1, Professional Paper, NASA Jet Propulsion Laboratory, 14 pp.

Andreae, M. O., 1995: *Future Climates of the World: World Survey of Climatology*, A. Henderson-Sellers Elsevier, Amsterdam, 16, pp. 341-392.

Christensen, J. H., 1997: The Danish Eulerian Hemispheric Model - A Three-Dimensional Air Pollution Model Used for the Arctic. *Atm. Env.*, 31, 4169-4191.

Chun,Y., J. Kim, J. C. Choi, K. O. Boo, S. N. Oh, M. Lee, 2001: Characteristic Number Size Distribution of Aerosol During Asian Dust Period in Korea. *Atmospheric Environment*, 35, 2715 -2721.

d'Almeida, G. A., P. Koepke, E. P. Shettle, 1991: *Atmospheric Aerosols, Global Climatology and Radiative Characteristics*. A. Deepak, 561 pp.

Deepak, A., and H. E. Gerber, Eds., 1983: *Report of the experts meeting on aerosols and their climatic effects*. World Meteorological Organization, WCP-55, 107 pp.

Goddard Space Flight Center, cited February 2007: MODIS Specifications. [Available online at http://modis.gsfc.nasa.gov/about/specifications.php].

Griffin, M. K., H. K. Burke, J. P. Kerekes, 2004: Understanding Radiative Transfer in the Midwave Infrared, a Precursor to Full Spectrum Atmospheric Compensation, *Proceedings of the SPIE, Vol. 5425,* edited by Sylvia S. Shen and Paul E. Lewis, 348-356.

Hegg, D. A., D. S. Covert, K. Crahan, H. Jonsson, 2002: The Dependence of Aerosol Light-Scattering on RH Over the Pacific Ocean, *Geophys. Res. Lett., 29(8)*, doi:10.1029/2001GL014495.

Hess, M., P. Koepke, and I. Schult, 1998*:* Optical Properties of Aerosols and Clouds: The Software Package OPAC. *Bulletin of American Meteorological Society*, 79, 831-844.

Husar, R,B., J. M. Prospero, and L. L. Stowe, 1997: Characterization of Tropospheric Aerosols Over the Oceans with the NOAA Advanced Very High Resolution Radiometer Optical depth Operational Product. *J. Geophys. Res., 102*, 16,889-16,909.

Husar, R. B., J. D. Husar and L. Martin, 2000: Distribution of Continental Surface Aerosol Extinction Based on Visual Range Data. *Atmos. Environ*. 34, 5067-5078.

Kidder, S. Q. and T. H. Vonder Haar, 1999: Satellite Meteorology: An Introduction. Academic Press, 466 pp.

Koepke, P., M. Hess, I. Schult, and E.P. Shettle, 1997: Global Aerosol Dataset, Report N 243, Max-Plank-Institut für Meteorologie, Hamburg, 44 pp.

Ming, Y., L. M. Russell, 2001: Predicted hygroscopic growth of sea salt aerosol, *J. Geophys. Res., 106(D22),* 28259-28274.

National Weather Service Climate Prediction Center, cited February 2007: Stratosphere Global Temperature Time Series. [Available online at http://www.cpc.ncep.noaa.gov/products/stratosphere/temperature/].

Navy Research Laboratory Monterey, CA, cited February 2007: Description of NAAPS (Navy Aerosol Analysis and Prediction System) Global Aerosol Model. [Available online at http://www.nrlmry.navy.mil/aerosol_web/Docs/globaer_model.html].

Navy Research Laboratory Monterey, CA, cited February 2007: Overview of NAAPS: Navy Aerosol Analysis and Prediction System. [Available online at http://www.nrlmry.navy.mil/aerosol_web/Docs/nrlmryonrprop.html].

Quenzel, H., and H. Müller, 1978: *Optical properties of single Mie particles: Diagrams of intensity-, extinction-, scattering-, and absorption efficiencies*. Universität München, Meteorologisches Institut, Wiss. Mit., 34, 59 pp.

Ramanathan, V., J.A. Coakley, Jr., 1978: Climate Modeling Through Radiative-Convective Models, *Review of Geophysics & Space Physics,* 16, p. 465.

Ramanathan, V, P. J. Crutzen, J. Lelieveld , A. P. Mitra, D. Althausen, J. Anderson, M. O. Andreae, W. Cantrell, G. R. Cass, C. E. Chung, *et al.,* 2001: Atmosphere: Aerosols, Climate, and the Hydrological Cycle**.** *J Geophys Res,* 106, 28371–28398.

Seinfeld, J. H., S. N. Pandis, 1998: *Atmospheric Chemistry and Physics, From Air Pollution to Climate Change.* John Wiley and Sons Inc., 1326 pp.

Shettle, E. P. and Fenn, R. W., 1979: *Models for the Aerosols of the Lower Atmosphere and the Effects of Humidity Variations on Their Optical Properties*. AFGL-TR-79-0214, ADA085951.

Smith, R.B., 2005: Computing the Planck Function, Professional Paper, Yale University.

Stephens, G. L., C. W. Paltridge, and C. M. R. Platt, 1978: Radiation profiles in extended water clouds III: Observations. *J. Atmos. Sci.,* 35, 2133–2141.

University Corporation for Atmospheric Research Cooperative Program for Operational Meteorology, Education and Training, cited February 2007: Dust Forecasting Module. [Available online at http://www.meted.ucar.edu/mesoprim/dust/frameset.htm].

University of Wisconsin, cited January 2007: Vis5D. [Available online at http://www.ssec.wisc.edu/~billh/vis5d.html].

Van de Hulst, H.C., 1981: Light scattering by small particles. *New York: Dover Publications,* 470 pp.

Vermote, E. F., N. El Saleoql, C.O. Justice, Y. J. Kaufman, J. L. Privette, L. Remer, J. C. Roger, and D. Tanre, 1997: Atmospheric Correction of Visible to Middle-Infrared EOS-MODIS Data Over Land Surfaces: Background, Operational Algorithm and Validation, *J. Geophys. Res., 102, (D14),* 17,131-17,141.

Westphal, D. L., O. B. Toon, and T. N. Carlson, 1988: A case study of mobilization and transport of Saharan dust. *J. Atmos. Sci*., 45, 2145-2175.

Westphal, D. L., 2000: Real-time Applications of a Global Multi-component Aerosol Model, Professional Paper, Submitted for publication in *J. Geophys. Res*.

Yuan, C. S., C. Sau, M. Chen, M. Huang, S. Chang, Y. Lin, and C. Lee, 2003: Mass Concentration and Size-Resolved Chemical Composition of Atmospheric Aerosols Sampled at the Pescadores Islands During Asian Dust Storm Periods in the Years of 2001 and 2002. TAO, Vol. 15, No. 5, 857-859.

THIS PAGE INTENTIONALLY LEFT BLANK

INITIAL DISTRIBUTION LIST

1. Defense Technical Information Center
   Ft. Belvoir, Virginia

2. Dudley Knox Library
   Naval Postgraduate School
   Monterey, California

3. AFCCC/DOO
   Asheville, North Carolina

4. Chairman, Code MR
   Department of Meteorology
   Naval Postgraduate School
   Monterey, California

5. Mr. Kurt Nielsen (Code MR/NE)
   Department of Meteorology
   Naval Postgraduate School
   Monterey, California

6. Dr. Andreas K. Goroch
   Marine Meteorology Division
   Naval Research Lab
   Monterey, California

7. Capt Paul W. Lucyk
   Castle Rock, Colorado